



3 1176 00096 2796

NACA RM L51K15



RESEARCH MEMORANDUM

THE EFFECTS OF SUCTION THROUGH POROUS LEADING-EDGE
SURFACES ON THE AERODYNAMIC CHARACTERISTICS OF A
47.5° SWEEPBACK WING-FUSELAGE COMBINATION

AT A REYNOLDS NUMBER OF 4.4×10^6

By Jerome Pasamanick and William I. Scallion

Langley Aeronautical Laboratory
Langley Field, Va.

CLASSIFICATION CANCELLED

Authority *NASA Res. Mem. #* Date *7-20-52*

RN-104

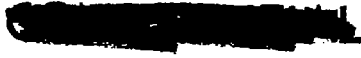
By *at 8-6-56* See

CLASSIFIED DOCUMENT

This material contains information affecting the National Defense of the United States within the meaning of the espionage laws, Title 18, U.S.C., Secs. 793 and 794, the transmission or revelation of which in any manner to an unauthorized person is prohibited by law.

NATIONAL ADVISORY COMMITTEE FOR AERONAUTICS

WASHINGTON
March 6, 1952


NACA LIBRARY
LANGLEY AERONAUTICAL LABORATORY
Langley Field, Va.

CONFIDENTIAL
NATIONAL ADVISORY COMMITTEE FOR AERONAUTICS

RESEARCH MEMORANDUM

THE EFFECTS OF SUCTION THROUGH POROUS LEADING-EDGE
SURFACES ON THE AERODYNAMIC CHARACTERISTICS OF A
47.5° SWEEPBACK WING-FUSELAGE COMBINATION
AT A REYNOLDS NUMBER OF 4.4×10^6

By Jerome Pasamanick and William I. Scallion

SUMMARY

The effects of suction through porous leading-edge surfaces on the longitudinal aerodynamic characteristics of a 47.5° sweptback wing-fuselage configuration have been investigated in the Langley full-scale tunnel at a Reynolds number of 4.4×10^6 . The wing section normal to the quarter-chord line was NACA 64₁All2, the aspect ratio was 3.4, and the taper ratio was 0.51.

The maximum lift coefficient of the model without suction was 0.98 and the configuration was longitudinally unstable. The application of area suction extending along 38.6 percent of the outboard wing span and from the zero to the 1-percent chordwise stations on the wing upper surface increased the maximum lift coefficient by 0.12 and reduced the drag, including the blower power drag, in the high lift range by approximately 30 percent. The model was longitudinally stable at the stall for this configuration; however, the stability at the stall was preceded by some erratic pitching characteristics. The configurations investigated having area suction along 19.3 percent and 57.9 percent of the outboard wing span resulted in longitudinal instability at the stall.

Of the range of the chordwise extent of area suction and flow coefficients investigated, stability at the stall was obtained only for suction between the zero percent and the 1-percent chordwise stations on the wing upper surface.

The initial application of suction at small removal flow rates resulted in large improvements in the lift and drag characteristics at the high angles of attack; however, the rate of improvement decreased and the effects approached a limiting value with increasing suction flow quantities.

Preliminary calculations indicate that the blower power drag at high lift coefficients with area suction would be lower than similar slotted configurations.

CONFIDENTIAL

INTRODUCTION

The inherently poor low-speed aerodynamic characteristics of thin highly sweptback wings may primarily be attributed to wing leading-edge air-flow separation. Studies have been made to evaluate the effectiveness of leading-edge flaps and suction slots as means for improving the characteristics of thin wings (references 1 to 5). In addition to the use of flaps and suction slots, the theory presented in reference 6 indicates that leading-edge separation on thin wings could be delayed by removing small quantities of air through porous leading-edge surfaces. Two-dimensional tests (reference 7) have shown improvements in the lift and drag characteristics of an airfoil, and the results reported in references 8 and 9 show the effect of area suction on the longitudinal stability characteristics of highly sweptback wings.

A research program has been underway at the Langley full-scale tunnel to study the low-speed aerodynamic characteristics of a swept-back wing-fuselage configuration with various combinations of high-lift flaps and boundary-layer control by suction. The longitudinal stability characteristics of the subject configuration were greatly improved with the use of either properly located leading-edge flaps or leading-edge spanwise suction slots; however, for the slots large suction-flow quantities were required to obtain any improvements. In view of the possibility of reducing the required suction quantities while still attaining improved air flow over thin wings, the program was extended to investigate the effects of area suction. The wing leading-edge sweep-back was 47.5° , the aspect ratio was 3.4, the taper ratio was 0.51, and the airfoil sections normal to the quarter-chord line were NACA 64₁A112.

The results include the effects of varying the extent of chordwise and spanwise area suction and suction-flow quantities on the maximum lift and longitudinal stability characteristics of the model at zero yaw. Forces, moments, and internal-suction pressures were measured for each configuration for a range of angle of attack through the stall. Surface pressure distributions were obtained for several configurations and angles of attack. The Reynolds number of the tests was 4.4×10^6 and corresponds to a Mach number of approximately 0.07.

COEFFICIENTS AND SYMBOLS

All results are presented in standard NACA form of coefficients and forces, and are referred to the wind axes. Moments are referred to the quarter-chord point of the mean aerodynamic chord.

C_L	lift coefficient (L/q_0S)
C_D	measured drag coefficient (D/q_0S)
C_{DE}	drag coefficient equivalent to blower power $(C_p C_Q \frac{S'}{S})$
C_m	pitching-moment coefficient $(M/q_0S\bar{c})$
C_Q	suction-flow coefficient (Q/V_0S')
C_p	pressure-loss coefficient $(\frac{H_0 - H_d}{q_0})$
P	pressure coefficient $(\frac{P - P_0}{q_0})$
L	lift, pounds
D	drag, pounds
M	pitching moment, positive when moment tends to increase angle of attack, foot-pounds
q_0	free-stream dynamic pressure, pounds per square foot $(\frac{1}{2}\rho_0 V_0^2)$
ρ_0	mass density of air, slugs per cubic foot
V_0	free-stream velocity, feet per second
S	total wing area, square feet
S'	wing area affected by span of area suction, square feet
c	wing chord, measured in plane perpendicular to quarter-chord line, feet
c'	wing chord, measured in plane parallel to plane of symmetry, feet
\bar{c}	wing mean aerodynamic chord, measured in plane parallel to plane of symmetry, feet $(\frac{2}{S} \int_0^{b/2} c'^2 dy)$

b	wing span, measured perpendicular to plane of symmetry, feet
y	distance measured perpendicular to plane of symmetry, feet
x	distance measured parallel to plane of symmetry, feet
Q	total quantity of flow through permeable surfaces, cubic feet per second
H ₀	free-stream total pressure, pounds per square foot
H _d	total pressure inside wing duct, pounds per square foot
p	local static pressure, pounds per square foot
p ₀	free-stream static pressure, pounds per square foot
R	Reynolds number ($\rho_0 V_0 \bar{c} / \mu$)
μ	coefficient of viscosity, slugs per foot-second
α	angle of attack of wing chord line, measured in plane of symmetry, degrees

MODEL

General dimensions of the model are given in figure 1, and a photograph of the model mounted in the Langley full-scale tunnel is presented as figure 2. The wing leading-edge sweepback was 47.5° ; the aspect ratio was 3.4; the taper ratio was 0.51; and the airfoil sections normal to the quarter-chord line were NACA 64₁A112. The wing panels had no twist or geometric dihedral and were mounted in a low midwing position at zero incidence on a circular fuselage.

Suction was applied at the wing leading edge through porous surfaces, extended spanwise from the 22.8-percent semispan station to the wing tip, and extended chordwise from 1.0-percent chord on the lower surface to 8-percent chord on the upper surface (fig. 3). By a method of sealing the porous surface, investigation of the various spanwise and chordwise configurations was possible. The air flow was induced into two spanwise chambers inside each wing panel divided at the 61.4-percent semispan station in order to obtain closer spanwise control, and was then ducted into a common plenum chamber located in the fuselage. Flow control was regulated by throttle valves installed in each duct leading

from the wing and by a free-air-bleed valve located on the fuselage. The suction was supplied by a high-speed centrifugal compressor driven by a variable-speed electric motor with the compressor air inlet connected to the fuselage plenum chamber and the air outlet ducted to the fuselage tail pipe. Suction-flow quantities were measured by thin flat-plate orifice meters in each wing duct, and wing-chamber static pressures were recorded from flush wall orifices. The pressure loss coefficients C_p were determined from total pressure measurements obtained at the junctures of the wing chambers and the air suction ducts. Airfoil surface pressures (measured in a plane parallel to the plane of symmetry) were measured over the left wing panel by flush static orifices located at four spanwise stations, as shown in table I.

DESIGN, CONSTRUCTION, AND OPERATION OF LEADING-EDGE SURFACES

The selection of porous surfaces for leading-edge suction necessitated the consideration of such factors as the suction-flow quantity, the fabrication and exterior finish of the surfaces, and the characteristics of the suction power unit. Since it is believed that the procedures followed in the selection of the porous material and the special techniques involved in the fabrication of the leading edges are noteworthy, the following operational methods developed during the present investigation are included.

The first step in the procedure used for the selection of the porous surfaces was to calculate the theoretical two-dimensional-airfoil pressure distribution for several section lift coefficients (reference 10). The assumption was then made that the internal suction pressure was at least equal to the peak negative pressure on the airfoil surface to prevent outflow and the resultant chordwise inflow or normal velocities were determined for materials having various grades of porosity. The chordwise normal velocities were integrated over the part of the chord involved to obtain the suction-flow quantities and it was found that, for a material having a porosity characteristic of 1-foot-per-second velocity normal to the surface at 0.25 pound per square inch or 7 inches of water-pressure drop across the surface, the suction-flow coefficients would vary between 0.00075 and 0.0025 as the chordwise extent of suction varied from 1 to 6 percent of the wing chord.

The next step was to select a suitable material which could be incorporated into the wing leading edge and meet the requirements for area suction. It was desirable to use a material which had a very large number of small openings, aerodynamically smooth, easily fabricated,

and also capable of being cleaned. Previous investigations of boundary-layer control by area suction have employed blotting paper, sintered bronze (reference 7), linen gauze (reference 8), and numerous screen and mesh combinations. An extensive study had been made by the Cascade Aerodynamics Section of the Langley Aeronautical Laboratory to determine the porosity characteristics and availability of a large variety of porous materials. The materials were tested in the basic condition as supplied by the manufacturers or processed either mechanically or chemically. From the findings of this search it was possible to select a porous material which would best serve the purpose of the present investigation. The material chosen was a metal filter cloth of monel wire which had a mesh of 700×80 wires per inch and total thickness of 0.0105 inch. The basic porosity characteristics of the material as received are given in figure 4. The material before processing was much too porous for the need of the present investigation; however, by decreasing the thickness of the filter cloth through a hammering procedure the desired porosity condition was obtained (fig. 4) and the surface roughness was reduced. Particular care and effort was exerted during this step because the hammering procedure is irreversible and the thickness and porosity of the material could be made nonuniform. The skin thickness after hammering ranged between 0.0071 and 0.0073 inch with little variation in porosity. The hammered filter cloth was bonded around the edges to a coarse spacer screen (0.024 inch thick) and attached to a perforated-steel back-up sheet (0.094 inch thick) formed to the contour of the airfoil. The total thickness of the porous surface and backing was approximately $1/8$ inch and the screen and back-up-sheet combination did not appreciably affect the porosity characteristics as determined for the metal filter cloth.

The extent of the chordwise and spanwise area suction was maintained by a strippable nonporous plastic coating which was carefully sprayed onto the surface. The plastic-coating thickness was approximately equivalent to the thickness of ordinary cellulose tape; however, the surfaces were sanded and the edges were feathered. In the process of spraying the plastic coating onto the surfaces some impregnation occurred and it was necessary to pass a solvent cleaner through the exposed surfaces immediately after a section was stripped. During the course of the investigation the surfaces were repeatedly cleaned with carbon tetrachloride in order to remove dust and other particles which clogged the material as a result of boundary-layer suction. The porosity of the material after it had been stripped of the coating and after it had been exposed to the air for the complete time of testing is presented in figure 4. It should be pointed out that the indicated loss in porosity represents the extreme limit but by repeated cleaning of the surfaces the porosity loss was recovered and most of the tests were conducted in the region representative of the clean condition (fig. 4).

TESTS AND RESULTS

Tests to determine the effects of leading-edge area suction on the longitudinal aerodynamic characteristics of the model were made in the Langley full-scale tunnel. Force data, internal-flow-pressure data, and airfoil pressure distributions were obtained at zero yaw over a range of angle of attack from small negative angles through the angle for maximum lift. The extent of the spanwise and chordwise length of exposed surface was varied from $0.228\frac{b}{2}$ to $1.00\frac{b}{2}$ and from zero chord to 0.06 chord on the upper surface, respectively, with suction flow coefficients varying between 0.0007 and 0.0035. The Reynolds number of the investigation was approximately 4.4×10^6 corresponding to a Mach number of 0.07.

The data have been corrected for jet-boundary effects (as determined from the straight-wing method of reference 11), blocking effects, stream alignment, and wing-support interference. In addition, a drag tare correction (which for most conditions was very small) has been applied to compensate for the effects of the air-jet thrust due to the blower operation. The drag coefficients C_D as presented in the figures are the measured coefficients of the external drag of the wing-fuselage combination and do not include the blower-power drag coefficients. The wing areas used in the computation of the blower-power drag coefficients are presented in table II.

A summary of the maximum-lift results and the longitudinal stability characteristics for the various configurations tested is presented in table III. In order to facilitate the discussion of results, the data are arranged in the following order of figures. The longitudinal aerodynamic characteristics of the basic wing are given in figure 5, and the airfoil pressure distributions are presented in figure 6. Figures 7 to 9 present force test data and airfoil pressure distributions to illustrate the effect of the spanwise variation of suction on the wing aerodynamic characteristics. The results of the chordwise variation of area suction are presented in figure 10, and the airfoil pressure distributions of the corresponding conditions are shown in figures 11 and 12. The effects of the suction-flow quantity on the wing longitudinal characteristics are given in figure 13. The results of the equivalent blower drag for the wing employing suction slots or porous surfaces are presented in figure 14.

DISCUSSION OF RESULTS

Basic Wing Characteristics

The longitudinal aerodynamic characteristics of the basic wing shown in figure 5 are similar to the results presented in reference 5. The maximum lift coefficient of the model without suction is 0.98 at an angle of attack of 22° and the configuration at this attitude is longitudinally unstable. In the low- and moderate-lift-coefficient range, up to a C_L of 0.8, $\alpha = 15^\circ$, the lift, drag, and pitching characteristics are very nearly linear. Increasing the angle of attack above 15° resulted in large increases in drag. Between angles of 15° and 17° the C_m curves indicate large increases in the nose-down pitching moments. These abrupt changes can be attributed to a "bubble" of air-flow separation occurring at the wing leading edge, which effectively alters the leading-edge profile, and produced a localized lift increase in the tip region and a rearward movement of the wing center of pressure. Although the leading-edge bubble is not located (fig. 6(c)), because of the lack of spanwise pressure distributions, it is estimated from the data of reference 5 to be between the 73- and 93-percent-span stations. The flow outboard of the disturbance although stalled produced some lift increase and figure 6(c) illustrates the region to be near the 93-percent-span station. The leading-edge disturbance progressed inboard with increasing angle of attack and at an angle of attack of 18.1° (fig. 6(d)) the phenomena had moved inboard to the 53-percent-span station. For this condition the decrease in lift over the outboard wing sections and the accompanying forward movement of the center of pressure resulted in longitudinal instability. The inboard progression of the leading-edge disturbance is also evident at an angle of attack of 20° (fig. 6(e)) ($\frac{2y}{b} = 0.34$).

Effect of Area Suction on the Longitudinal Characteristics

Spanwise extent of suction.- The control of the air flow over the outboard sections of highly sweptback wings can be attained with properly designed leading-edge flaps, slats, or suction. In each case, however, there is a critical span required to produce longitudinal stability. The results of the spanwise variation of suction through porous surfaces for the present investigation are shown in table III and representative curves are presented in figure 7. It can be seen from figure 7 that the application of suction to the largest value of C_Q obtained along 1 percent of the wing chord and the outboard 19.3 percent of the wing span has a negligible effect on the maximum lift coefficient

($C_{L_{max}}$ did occur 2° earlier) and results in a small reduction of drag between C_L of 0.8 and the maximum lift coefficient. The pitching-moment characteristics just prior to $C_{L_{max}}$ are greatly influenced by this suction although the model was longitudinally unstable beyond $C_{L_{max}}$. The abrupt pitching-moment changes which were present for the basic wing without suction were eliminated and the model became neutrally stable up to and including the angle of attack for $C_{L_{max}}$. It was previously pointed out for the basic wing that a bubble of separation at the outboard leading edge resulted in a rearward movement of the center of pressure and an accompanying increase in stability. Suction spanning the outboard $0.19\frac{b}{2}$, and with a $C_Q = 0.00125$, eliminated the separation bubble and delayed the stall to higher angles of attack, until all sections on the outboard half of the wing span stalled in unison. The changes in lift over the outboard 19-percent wing span cannot be detected from the lift data, but the pitching moments clearly show the beneficial effects of suction.

The extension of area suction to the outboard 38.6 percent of the wing span resulted in an increase in the maximum lift coefficient to 1.10 ($\Delta C_{L_{max}} = 0.12$). The drag coefficients in the range near $C_{L_{max}}$ were unaffected by the application of suction. The pitching moments at the maximum lift coefficient were longitudinally stable. In the lift-coefficient range between 0.96 and 1.04, the data indicated an abrupt increase in negative pitching moment followed by a recovery to the initial moment. The airfoil-pressure diagrams of figure 8(d) show a disturbance occurring in the region of the 53-percent-span station and extending outboard to the 73-percent-span station. (Compare figs. 8(c) and 8(d).) The pressures are also somewhat affected inboard of the 53-percent-span station but not so noticeably as the pressures at the outboard stations. The effect of the disturbance was to shift the center of pressure rearward with respect to the moment axis and produce a nose-down pitching moment. A further increase in angle of attack (fig. 8(e)) resulted in a loss of lift in the region near the 53-percent-span station which is inboard of the extent of area suction ($0.61\frac{b}{2}$ to $1.00\frac{b}{2}$). The peak negative pressures at the wing tip were reduced and trailing-edge separation occurs at the outboard stations for this angle of attack, $\alpha = 20^\circ$. The pitching-moment curve at this attitude reversed and indicates a nose-up tendency. Near the maximum lift coefficient (fig. 8(f)), the flow over the wing tip sections and the sections inboard of the area suction were stalled. The unstalled wing areas in the region of the 73-percent span station are sufficiently behind the moment axis to produce a net stabilizing effect. It is possible that, if the optimum span of area suction or greater flow quantities were obtained, the slightly

erratic pitching characteristics encountered prior to the stable break at the maximum lift would have been eliminated.

Additional increase in spanwise extent of suction (table III and fig. 7) had no appreciable effects on the lift characteristics of the model such as were obtained for the wing with suction spanning the outboard 38.6 percent of the wing. In the moderate and high lift-coefficient range, however, the drag coefficients including the blower power drag were reduced by 15 to 35 percent. The longitudinal stability characteristics were similar to those for the basic wing, with the exception that the nose-down pitching moments prior to the instability at the stall, were not so pronounced. The pressure diagrams given in figure 9 show that unstalled flow was maintained over the wing leading edge to high angles of attack and that initial separation occurred at the trailing parts of the outboard wing sections. At an angle of attack of 20° the model exhibited an abrupt diving tendency. The pressure diagrams of figure 9(e) show that the leading-edge disturbance occurred along the outboard sections and produced the nose-down condition. Higher angles of attack resulted in a wing stall similar to that obtained with a large span leading-edge flap or for the basic wing, that is, stall originating at the wing tips and progressing inboard.

Chordwise extent of suction.- The chordwise extent of area suction which produced longitudinal stability at the stall and gave the largest increment in maximum lift was found to be between the zero-percent-chord station and the 1-percent-chord station on the wing upper surface (table III and fig. 10). The investigation of reference 5 showed very similar results with a suction slot located at the one-half-percent-chord station. The data of figure 10 show the largest increments in maximum lift to be 0.12 and 0.15 for the 1-percent-chordwise configuration spanning 38.6 percent and 77.2 percent of the outboard wing panels, respectively. Extending the suction surface to the $2\frac{1}{2}$ - or 3-percent-chord stations, upper surface, resulted in maximum lift coefficients of 0.08 lower than that obtained for the smaller opening configuration having the same flow coefficients. The reduction in lift is probably due to the smaller normal inflow velocities since the suction-flow quantities were essentially the same; whereas the chordwise extent of area suction was increased. Some of the configurations (table III) were compared on the basis of equal average normal velocities, but these showed that $C_{L_{max}}$ was approximately 0.06 lower than that obtained for the smaller opening configuration. Another factor which may contribute to the smaller increment of lift could be the reduced normal inflow velocities at the region of the peak negative pressure for the larger chordwise extent of suction as compared to the smaller chordwise extent of suction even if the average normal velocities were the same for both configurations. The leading-edge surfaces were of a uniform porosity and the internal suction pressure was of a constant value for each

attitude; therefore, the chordwise inflow velocities increased as the open surface progressed further back from the wing leading edge. At an angle of attack approaching the maximum lift, the peak negative airfoil pressure was at, or very near, the zero-percent-chord station. It has been previously pointed out that, for boundary-layer control to be effective, it is of prime significance to apply suction in the vicinity of the onset of the steep adverse pressure gradient. The results of the investigation of a sweptback wing at low Reynolds numbers (reference 9) substantiate the fact that area suction over small parts of the airfoil in the region of the peak negative pressures would produce the highest values of $C_{L_{max}}$ for given suction-flow rates and less power would be required to obtain a given maximum lift than if area suction was extended rearward on the airfoil. A comparison of the pressure diagrams in figures 8 and 11 shows the inadequacy of the larger chord area suction at the highest C_Q obtained for eliminating the leading-edge disturbances over the affected sections. In the region of the 73-percent-span station at an angle of attack of 20° , (figs. 8(e) and 11(e)) indicate the flow to be stalled for the configuration having porous surfaces extending to the $2\frac{1}{2}$ -percent-chord station. At an angle of attack of 24° , most of the wing was stalled for the larger chordwise extent of area suction; however, a small region of unstalled flow existed at the wing leading edge between the 73-percent-span station and the wing tip.

In the lift range prior to $C_{L_{max}}$ the drag coefficients increased as the chordwise extent of area suction increased but at $C_{L_{max}}$ the drag coefficients, including the blower power drag, (regardless of the chordwise extent of suction) were about the same as the basic wing drag. The longitudinal stability characteristics were similar to the characteristics of the basic wing. The configuration which was previously stable, 38.6-percent wing span, became unstable when the chord of suction was extended rearward.

Several tests were made to determine the effects of opening the porous surface from 0.005c to 0.045c wing upper surface and the results are shown in table III and figures 10 and 12. These data show the wing aerodynamic characteristics to be essentially unaffected by suction in that region.

Suction-flow rates.— The improvements in the longitudinal aerodynamic characteristics of the model with increasing suction-flow quantities are similar to the findings reported in references 7 and 8. The initial application of suction having small removal flow rates resulted in large beneficial effects on the lift, drag, and pitching-moment characteristics. An increase in the suction-flow quantities did not proportionally improve the wing aerodynamic characteristics but reached a

point of no net gains. The effect of increasing the suction-flow quantities from $C_Q = 0.00067$ to $C_Q = 0.00092$ (fig. 13(a)) were negligible on the lift and drag characteristics of the model with the outboard 38.6-percent span of the wing leading edge porous from the zero to the 1-percent-chord stations. The pitching-moment characteristics with the smaller boundary-layer-removal quantity $C_Q = 0.00067$ were stable up to the maximum lift followed by an abrupt unstable condition. The larger flow rate $C_Q = 0.00092$ produced a longitudinally stable configuration at the stall and it is possible that, if data were obtained with greater suction quantities, the break in the pitching-moment curve prior to the stall could have been eliminated.

The wing configurations having larger spanwise and chordwise porous surfaces show large drag reductions at moderate and high lift coefficients (figs. 13(b) and 13(c)). The reduction in drag, including blower power drag, was approximately 35 percent in the lift range near $C_{L_{max}}$ and for the conditions utilizing very large boundary-layer-removal quantities the drag coefficients were reduced by more than 20 percent. Although the blower power drag coefficient is directly proportional to the suction-flow rate and pressure-loss coefficients, in this investigation the flow rate was predominant in determining the power drag because the rate of increase of the pressure-loss coefficient was not so great as the rate of increase of the suction-flow coefficient. If the porous material used in the fabrication of the leading edges had been less dense, it is possible that the drag coefficients in the lift range prior to the stall would have been lower than the drag values herein obtained, including the blower power drag.

The pitching-moment characteristics were improved with increasing suction-flow rate up to the stall for the wing configurations investigated. A small suction-flow rate resulted in a large improvement in the stability characteristics but increases in flow rate did not correspondingly improve the stability characteristics. The unstable pitching-moment break at the maximum lift coefficient occurred for all suction-flow rates with the exception of the configuration employing 38.6 percent-outboard span suction from the zero to the 1 percent chordwise stations. It is, therefore, apparent that in the present investigation the longitudinal stability characteristics of the model near $C_{L_{max}}$ are closely dependent upon the spanwise and chordwise extent of the porous surfaces.

BLOWER POWER DRAG COMPARISON OF TWO SPANWISE
SUCTION SLOTS AND POROUS SURFACES

The suction power required to induce the flow into a slot or through a porous surface was calculated from the relationship that the equivalent drag was directly proportional to the pressure-loss and suction-flow coefficients. This method of accounting for the suction power is acceptable if it is assumed that the efficiency of the suction system and the main propulsive system of the airplane are equivalent. The data required to calculate the blower power drag of the model with leading-edge suction slots were obtained from reference 5 and are presented herein in figure 14 with similar wing configurations having porous surfaces. The configurations for which the blower power drag was estimated are not directly comparable inasmuch as differences can be seen in the pitching-moment characteristics; however, each configuration represents the best that was obtained in the investigations. It should be noted that the power drag as presented in figure 14 is only applicable to the given conditions and any variation in the geometric characteristics of either the slots or porous surfaces would greatly influence the blower power drag coefficients.

The blower power drag coefficients for the smaller span porous suction configuration were increased slightly with increasing angle of attack to a value of 0.014 (fig. 14). The larger span area suction configuration, $0.772\frac{b}{2}$ showed a similar increase of C_{DE} with angle of attack until a maximum value of blower power drag (0.052) was obtained at $\alpha = 18^\circ$. The flow coefficients for the porous surface-wing configurations were constant throughout the angle-of-attack range and the pressure loss coefficients required to obtain these flow coefficients were only slightly influenced by the variation of the airfoil surface pressures. The pressure drop through the porous surfaces was more than 2 to 3 times greater than the value of the peak negative airfoil pressure. For the suction-slot configurations, the blower power drag coefficients varied irregularly with angle of attack. The pressure-loss coefficients were closely associated with the airfoil surface pressures in the region of the suction slots due to the small pressure drop through the slots. In the high angle-of-attack range the blower power drag for the suction-slot configurations was greater than the 77.2-percent and 38.6-percent-span-area suction configurations, respectively. In the present investigation, the maximum flow coefficient for the given configurations was about 0.0016 and the pressure-loss coefficient was 40. The maximum flow coefficient encountered for the wing with slots (reference 5) was approximately 0.035 and the pressure-loss coefficient was 10.

SUMMARY OF RESULTS

The results of the investigation in the Langley full-scale tunnel of the effects of leading-edge suction through porous surfaces on the aerodynamic characteristics of a 47.5° sweptback wing are summarized as follows:

1. Boundary-layer control, in general, improved the pitching-moment curve below the maximum lift coefficient and, for the configuration having suction spanning the outboard 38.6 percent of the wing span, the wing was longitudinally stable at the stall; however, the stability at the stall was preceded by some erratic pitching characteristics. The 19.3 percent and 57.9 percent spanwise suction configurations produced unstable pitching characteristics at the stall.

2. Of the range of the chordwise extent of area suction and flow coefficients investigated, stability at the stall was obtained only for suction between the zero percent and the 1-percent chordwise stations on the wing upper surface.

3. Leading-edge boundary-layer control applied over the outboard 38.6 percent of the wing span increased the maximum lift coefficient of the model from 0.98 to 1.10 and reduced the model drag, including the blower-power drag, by approximately 30 percent in the high-lift range.

4. Area suction at high angles of attack improved the lift and drag characteristics. The rate of improvement decreased and the effects approached a maximum value as the suction quantities increased.

5. Preliminary calculations indicate that the blower-power drag at high-lift coefficients with area suction would be less than that with the suction slot arrangement previously investigated on the same model configuration.

Langley Aeronautical Laboratory
National Advisory Committee for Aeronautics
Langley Field, Va.

REFERENCES

1. Foster, Gerald V., and Fitzpatrick, James E.: Longitudinal-Stability Investigation of High-Lift and Stall-Control Devices on a 52° Swept-back Wing with and without Fuselage and Horizontal Tail at a Reynolds Number of 6.8×10^6 . NACA RM L8I08, 1948.
2. Pasamanick, Jerome, and Sellers, Thomas B.: Low-Speed Investigation of Leading-Edge and Trailing-Edge Flaps on a 47.5° Sweptback Wing of Aspect Ratio 3.4 at a Reynolds Number of 4.4×10^6 . NACA RM L50E02, 1950.
3. McCormack, Gerald M., and Cook, Woodrow L.: Effects of Boundary-Layer Control on the Longitudinal Characteristics of a 45° Swept-Forward Wing-Fuselage Combination. NACA RM A9K02a, 1950.
4. McCullough, George B., and Gault, Donald E.: An Experimental Investigation of an NACA 64₁-012 Airfoil Section with Leading-Edge Suction Slots. NACA TN 1683, 1948.
5. Pasamanick, Jerome, and Sellers, Thomas B.: Full-Scale Investigation of Boundary-Layer Control by Suction through Leading-Edge Slots on a Wing-Fuselage Configuration Having 47.5° Leading-Edge Sweep with and without Flaps. NACA RM L50B15, 1950.
6. Thwaites, B.: A Theoretical Discussion of High-Lift Aerofoils with Leading-Edge Porous Suction. R. & M. No. 2242, British A.R.C., 1946.
7. Nuber, Robert J., and Needham, James R., Jr.: Exploratory Wind-Tunnel Investigation of the Effectiveness of Area Suction in Eliminating Leading-Edge Separation over an NACA 64₁A212 Airfoil. NACA TN 1741, 1948.
8. Cook, Woodrow L., Griffin, Roy N., Jr., and McCormack, Gerald M.: The Use of Area Suction for the Purpose of Delaying Separation of Air Flow at the Leading Edge of a 63° Swept-Back Wing. NACA RM A50H09, 1950.
9. Poppleton, E. D.: Wind Tunnel Tests on a Swept Back Wing Having Distributed Suction on the Leading Edge. TN No. Aero 2081, British R.A.E., Nov. 1950.
10. Abbott, Ira H., Von Doenhoff, Albert E., and Stivers, Louis J., Jr.: Summary of Airfoil Data. NACA Rep. 824, 1945. (Formerly NACA ACR L5C05.)

11. Theodorsen, Thoedore, and Silverstein, Abe: Experimental Verification of the Theory of Wind-Tunnel Boundary Interference. NACA Rep. 478, 1934.

TABLE I

AIRFOIL ORIFICE LOCATION

Chordwise station x/c'	
Upper surface	Lower surface
0	0
.005	.005
.010	.010
.015	.015
.025	.025
.040	.040
.060	-----
.080	-----
.120	-----
.170	.170
.220	-----
.320	.320
.420	-----
.520	.520
.620	-----
.720	.720

TABLE II

WING AREA AFFECTED BY POROUS LEADING-EDGE SURFACES

Span of porous material (percent $b/2$)	Wing area behind porous material S' (sq ft)	$\frac{S'}{S}$
80.7 - 100	32.82	0.145
61.4 - 100	71.10	.315
42.1 - 100	113.70	.503
22.8 - 100	163.72	.725


 NACA

TABLE III

SUMMARY OF MAXIMUM-LIFT RESULTS AND LONGITUDINAL
STABILITY CHARACTERISTICS

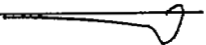
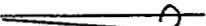
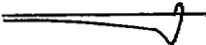
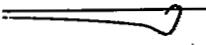
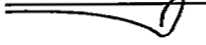
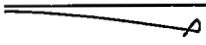
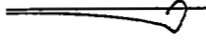
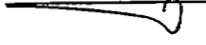
Spanwise location of porous material from q_c model (percent b/2)	Chordwise location (percent chord)	C_Q	$C_{L_{max}}$	$\Delta C_{L_{max}}$ (suction)	α at $C_{L_{max}}$ (deg)	Stability C_m against C_L
Sealed	-----	-----	0.98	----	22	
80.7 - 100	0 to 1	0.00064	1.00	0.02	22	
80.7 - 100	0 to 1	.00125	.98	----	20	
80.7 - 100	$\frac{1}{2}$ to $2\frac{1}{2}$.00159	.99	.01	22	
80.7 - 100	$\frac{1}{2}$ to $3\frac{1}{2}$.0015	.99	.01	22	
80.7 - 100	$\frac{1}{2}$ to $3\frac{1}{2}$	Suction power failure	.97	-.01	22	
61.4 - 100	0 to 1	.00067	1.09	.11	23.8	
61.4 - 100	0 to 1	.00092	1.10	.12	24.8	
61.4 - 100	0 to $2\frac{1}{2}$.0007	1.01	.03	22	
61.4 - 100	0 to $2\frac{1}{2}$.00123	1.00	.02	22	
61.4 - 100	0 to $4\frac{1}{2}$.00074	.99	.01	21	
61.4 - 100	0 to $4\frac{1}{2}$.00201	1.03	.05	21.9	
61.4 - 100	$\frac{1}{2}$ to $3\frac{1}{2}$.002	1.00	.02	22	

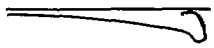
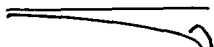
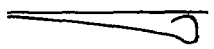
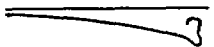
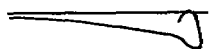
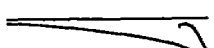
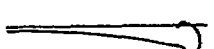
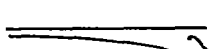
TABLE III

SUMMARY OF MAXIMUM-LIFT RESULTS AND LONGITUDINAL
STABILITY CHARACTERISTICS - Continued

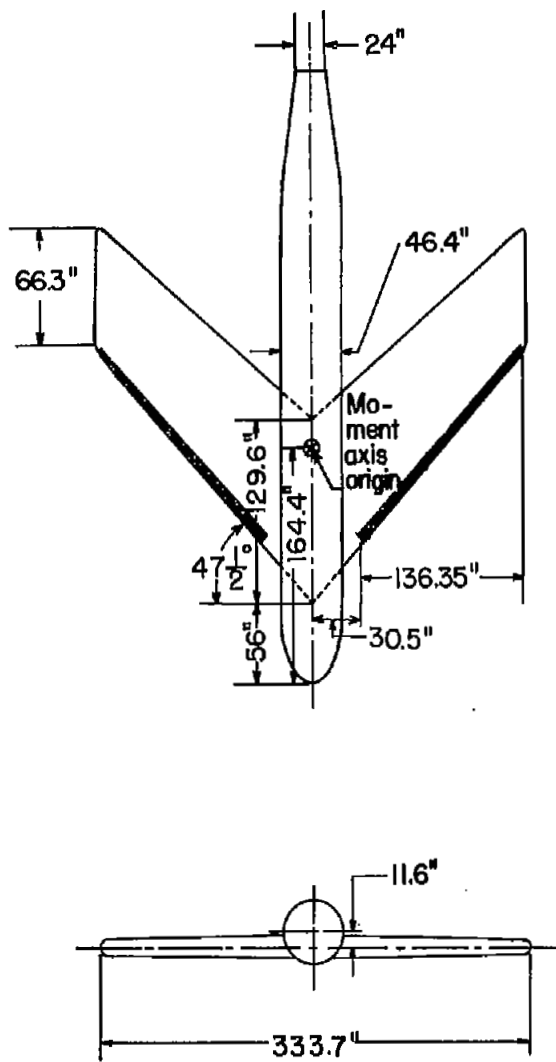
Spanwise location of porous material from \bar{c} model (percent $b/2$)	Chordwise location (percent chord)	C_q	$C_{L_{max}}$	$\Delta C_{L_{max}}$ (suction)	α at $C_{L_{max}}$ (deg)	Stability C_m against C_L
61.4 - 100	0 to $\frac{1}{2}$	0.00204	0.99	0.01	22	
42.1 - 61.4 61.4 - 100	0 to 1	.00201 .00093	1.09	.11	24.9	
42.1 - 61.4 61.4 - 100	0 to 1	.00244 .00126	1.08	.10	24.9	
42.1 - 61.4 61.4 - 100	$\frac{1}{4}$ to 3 to $\frac{1}{2}$.00288 .00204	1.00	.02	22	
22.8 - 61.4 61.4 - 100	0 to 1	.00119 .0008	1.13	.15	23.8	
22.8 - 61.4 61.4 - 100	0 to 1	.00186 .00123	1.15	.17	24.7	
22.8 - 61.4 61.4 - 100	0 to 1 0 to 2	.00093 .00083	1.09	.11	21.8	
22.8 - 61.4 61.4 - 100	0 to 1 0 to 2	.00191 .00165	1.12	.14	22.8	
22.8 - 61.4 61.4 - 100	0 to 2	.00093 .00068	1.06	.08	21.9	
22.8 - 61.4 61.4 - 100	0 to 2	.00269 .00199	1.14	.16	22.8	
22.8 - 61.4 61.4 - 100	0 to 2 0 to 3	.00266 .00201	1.13	.15	22.8	

TABLE III

SUMMARY OF MAXIMUM-LIFT RESULTS AND LONGITUDINAL
STABILITY CHARACTERISTICS - Concluded

Spanwise location of porous material from q_c model (percent $b/2$)	Chordwise location (percent chord)	C_Q	$C_{L_{max}}$	$\Delta C_{L_{max}}$ (suction)	α at $C_{L_{max}}$ (deg)	Stability C_m against C_L
22.8 - 61.4 61.4 - 100	0 to 3	0.00118 .0009	1.05	0.07	20.9	
22.8 - 61.4 61.4 - 100	0 to 3	.00269 .002	1.15	.17	22.8	
22.8 - 61.4 61.4 - 100	0 to 3 0 to $4\frac{1}{2}$.00119 .00093	1.04	.06	20.9	
22.8 - 61.4 61.4 - 100	0 to 3 0 to $4\frac{1}{2}$.0034 .00253	1.12	.14	23.8	
22.8 - 61.4 61.4 - 100	0 to $4\frac{1}{2}$.00123 .00093	1.03	.05	20.9	
22.8 - 61.4 61.4 - 100	0 to $4\frac{1}{2}$.00353 .00254	1.13	.15	22.8	
22.8 - 61.4 61.4 - 100	0 to $4\frac{1}{2}$ 0 to 6	.00121 .00091	1.02	.04	20.9	
22.8 - 61.4 61.4 - 100	0 to $4\frac{1}{2}$ 0 to 6	.00341 .00254	1.12	.14	21.8	
22.8 - 61.4 61.4 - 100	0 to 6	.00112 .00094	1.02	.04	22.9	
22.8 - 61.4 61.4 - 100	0 to 6	.00341 .00253	1.10	.12	20.8	





Wing area	225.98 sq ft
Aspect ratio	3.4
Taper ratio	0.51
Airfoil section	NACA 64, A112
Root chord	10.8 ft
Tip chord	55 ft
\bar{c}	8.78 ft

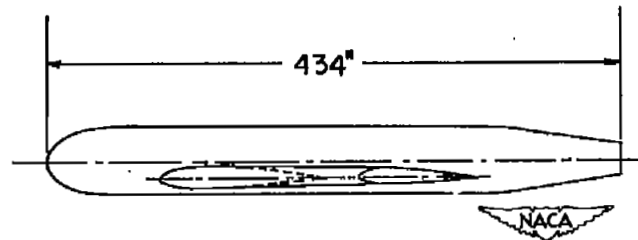


Figure 1.- Three-view drawing of a 47.5° sweptback wing-fuselage combination with boundary-layer control.

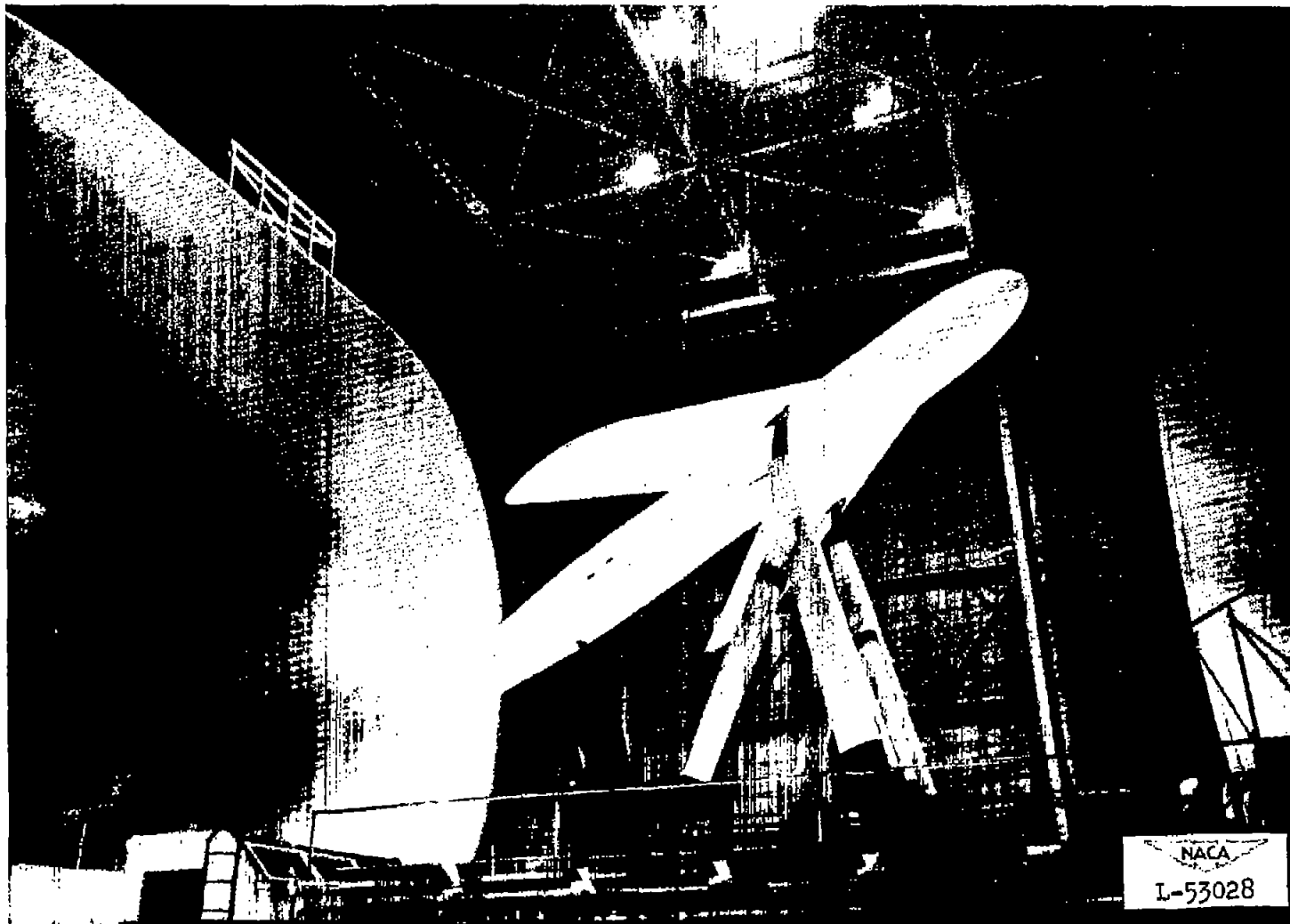
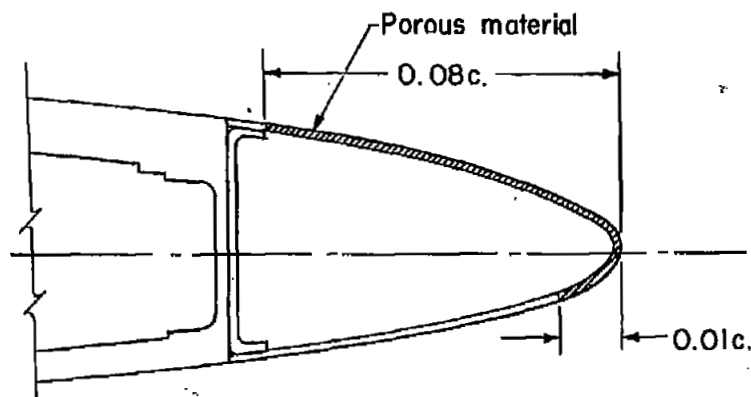
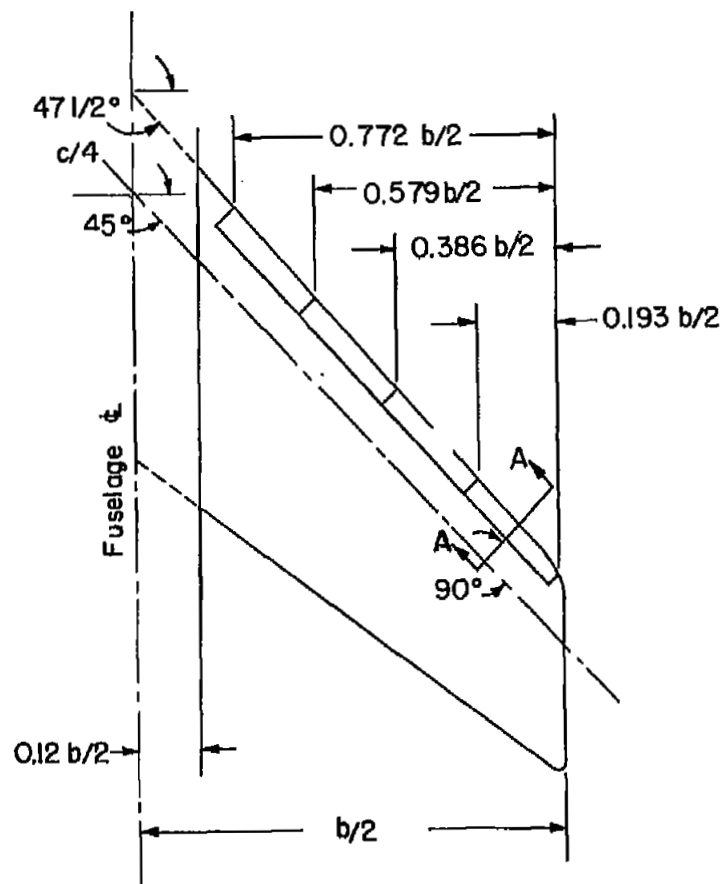


Figure 2.- Three-quarter front views of the 47.5° sweptback wing boundary-layer-control model mounted in the Langley full-scale tunnel.



(b) Enlarged view of section A-A

Figure 3.- The location and detail dimensions of porous leading-edge surfaces.



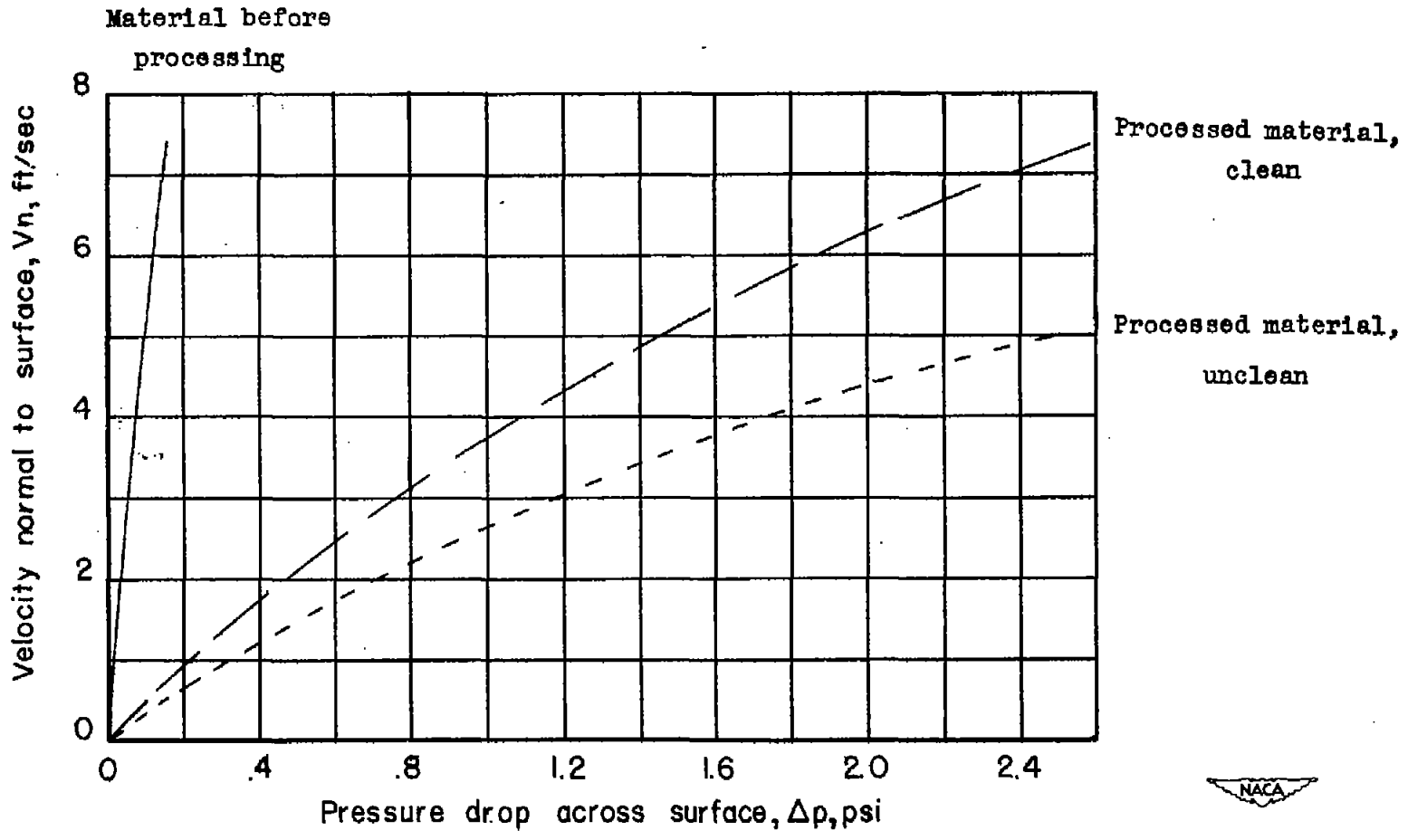


Figure 4.- Porosity characteristics of metal filter cloth.

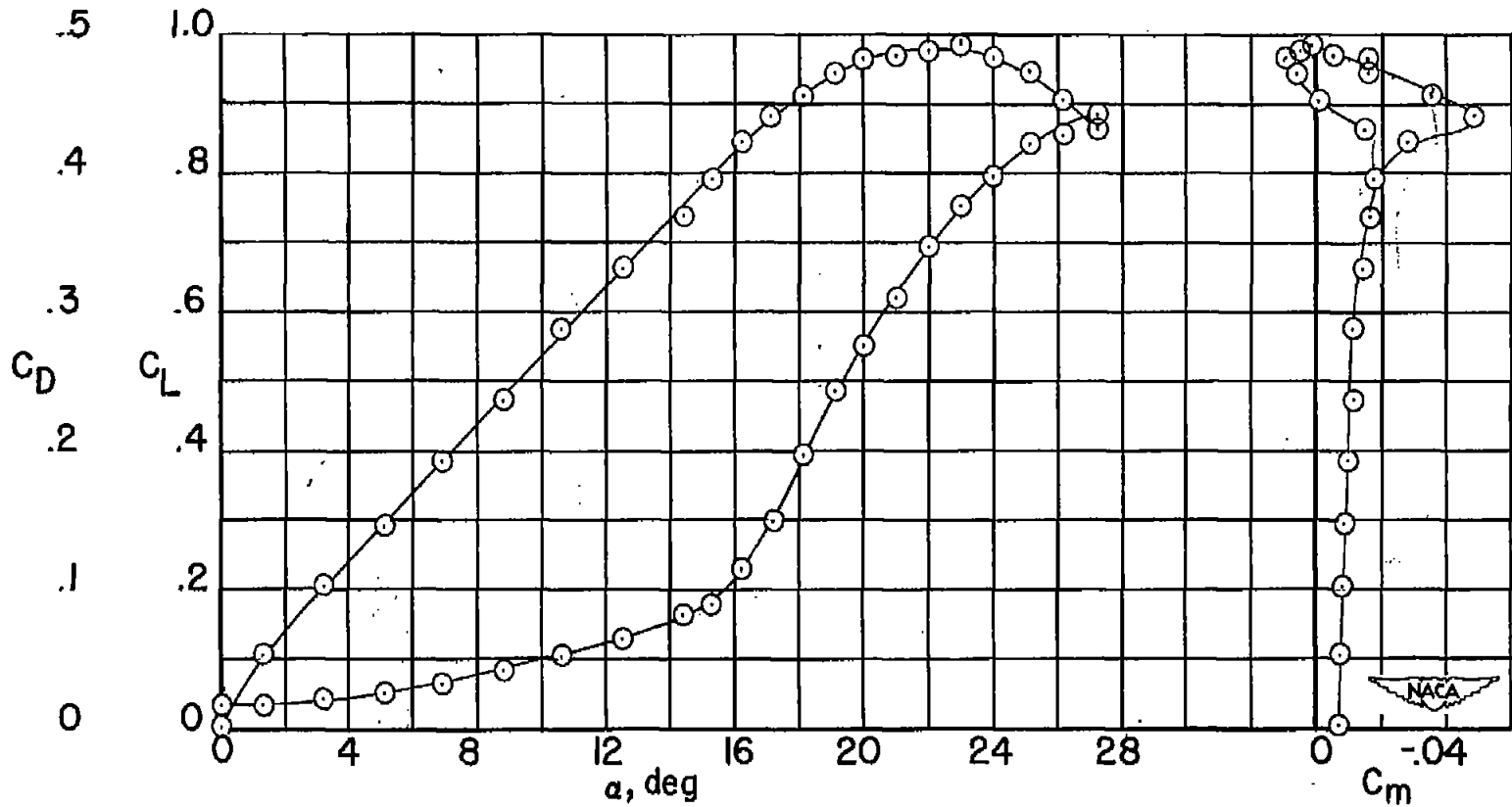
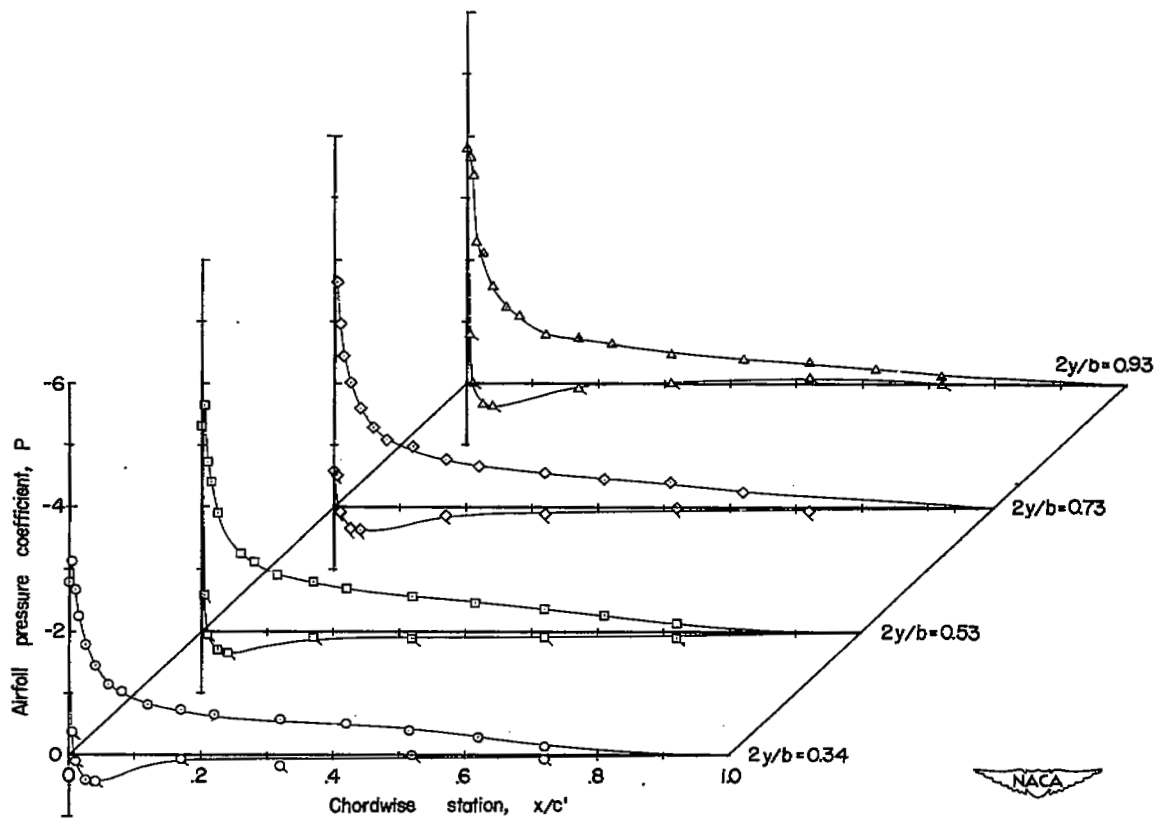
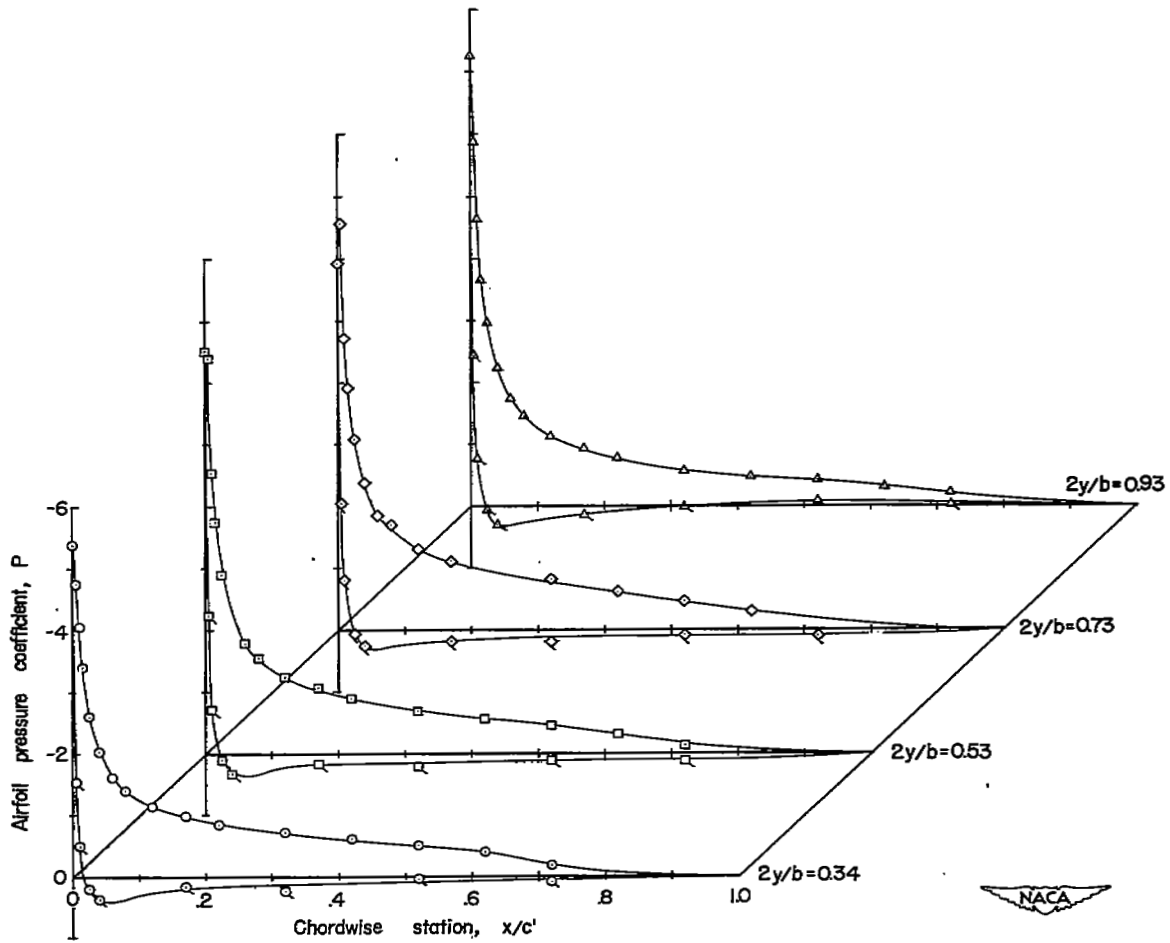


Figure 5.- Longitudinal aerodynamic characteristics of the 47.5° sweptback wing-fuselage combination. Porous surfaces sealed. $R = 4.4 \times 10^6$.



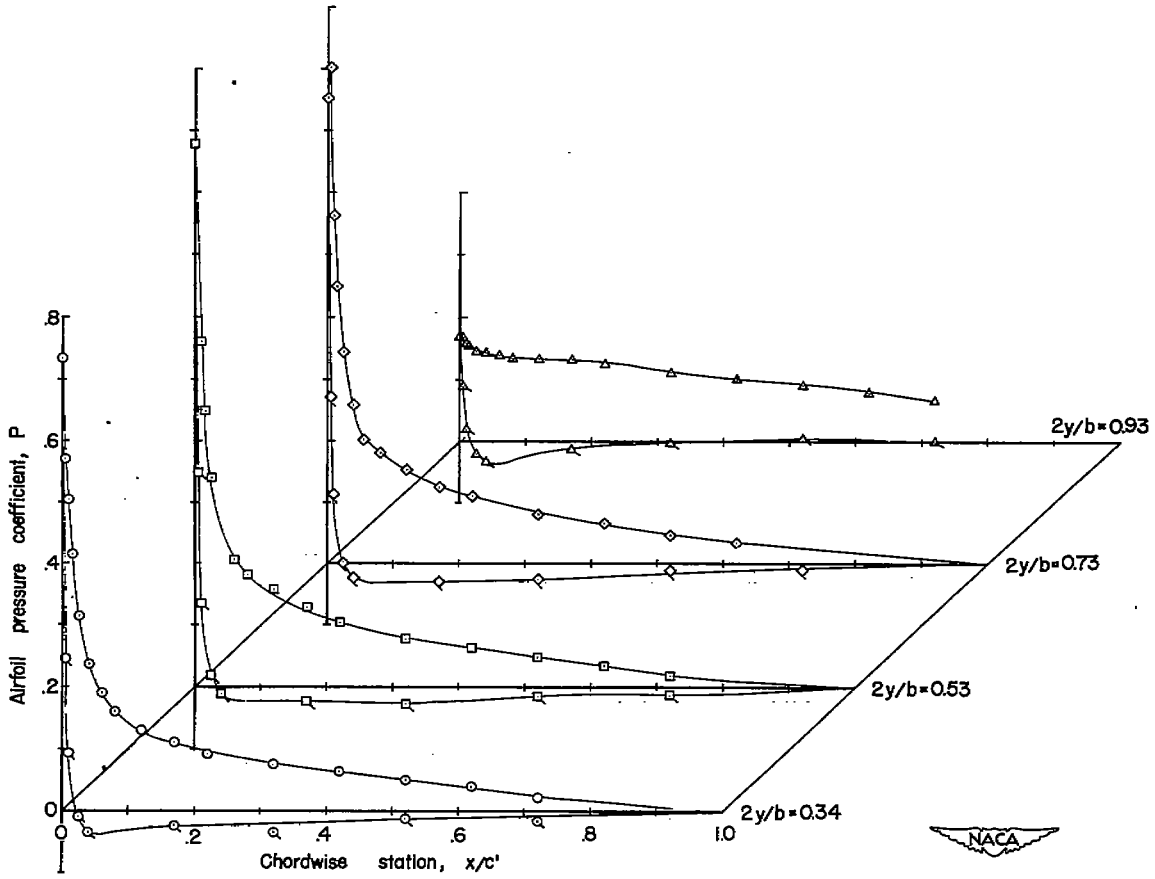
(a) $\alpha = 10.6^\circ$.

Figure 6.- Airfoil pressure distribution over a 47.5° sweptback wing. Porous surfaces sealed. $R = 4.4 \times 10^6$.



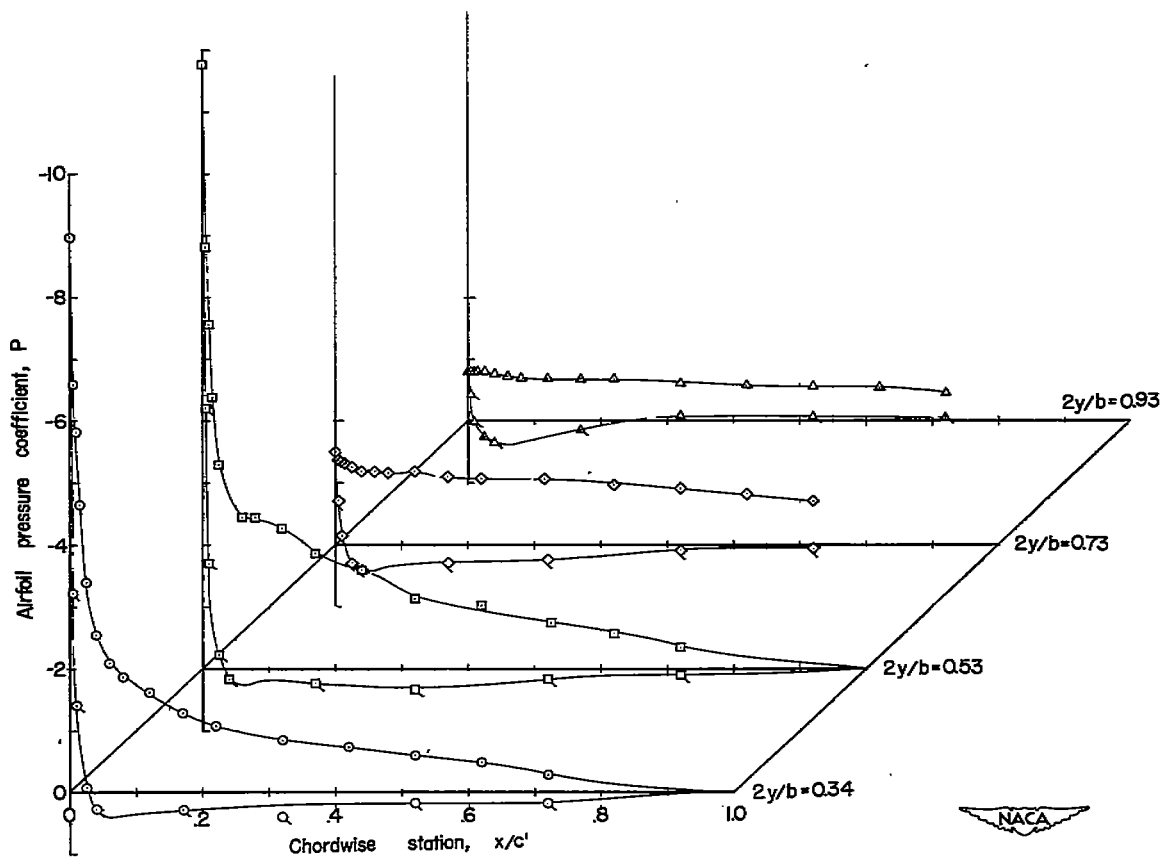
(b) $\alpha = 14.4^\circ$.

Figure 6.- Continued.



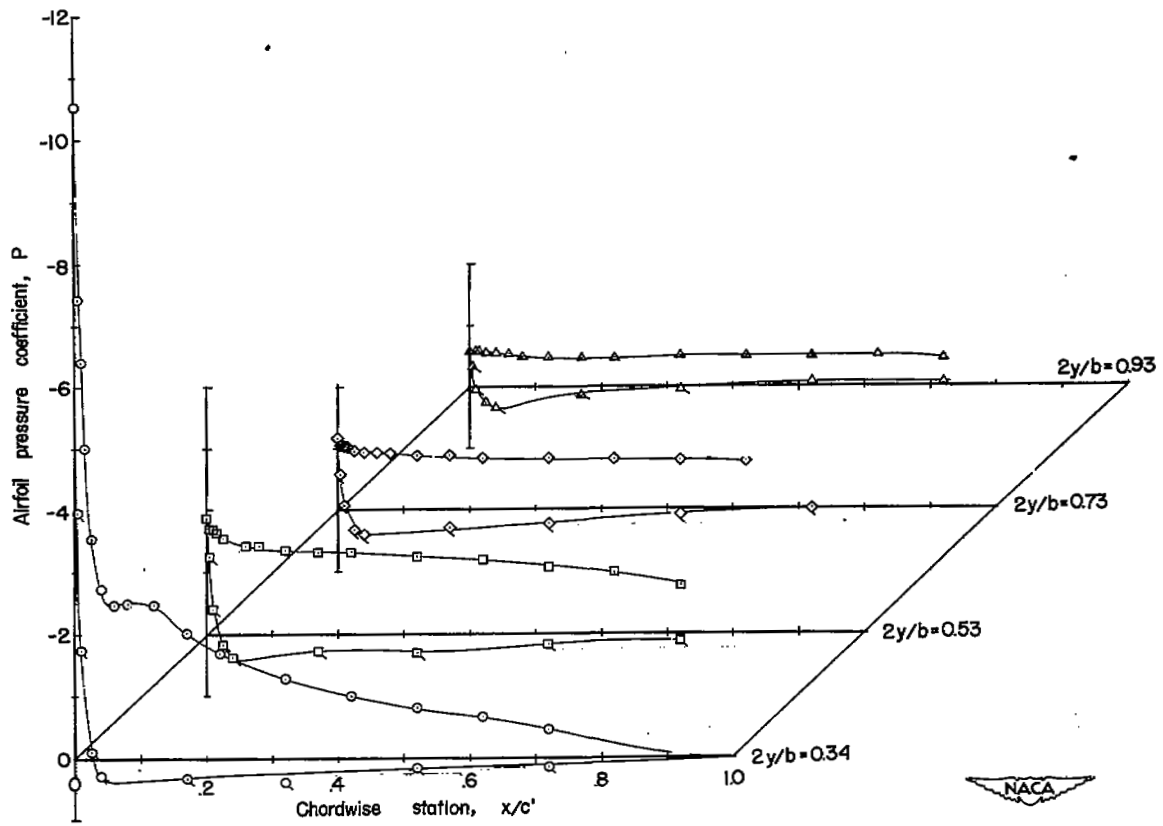
(c) $\alpha = 16.2^\circ$.

Figure 6.- Continued.



(d) $\alpha = 18.1^\circ$.

Figure 6.- Continued.



(e) $\alpha = 20^\circ$.

Figure 6.- Concluded.

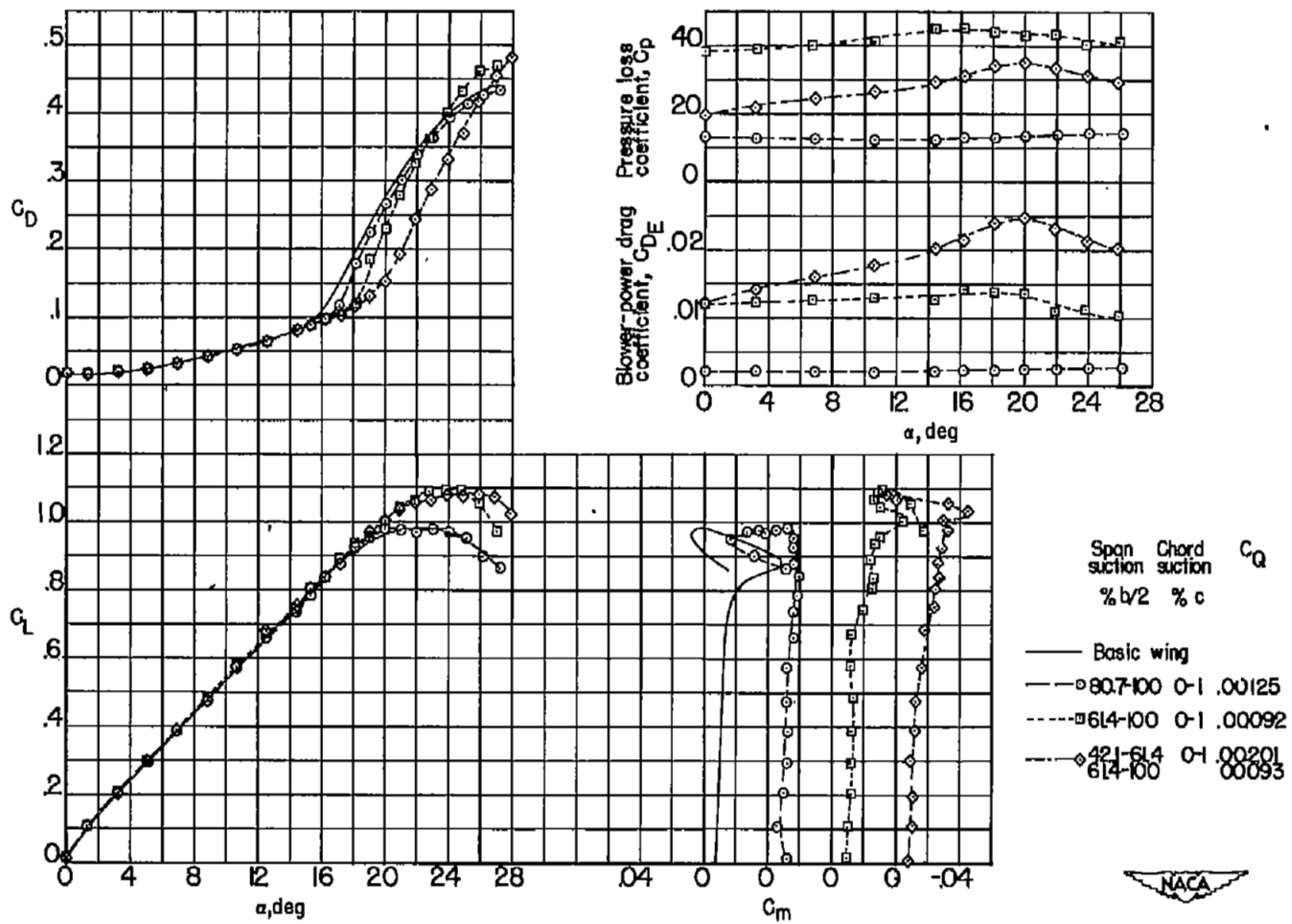
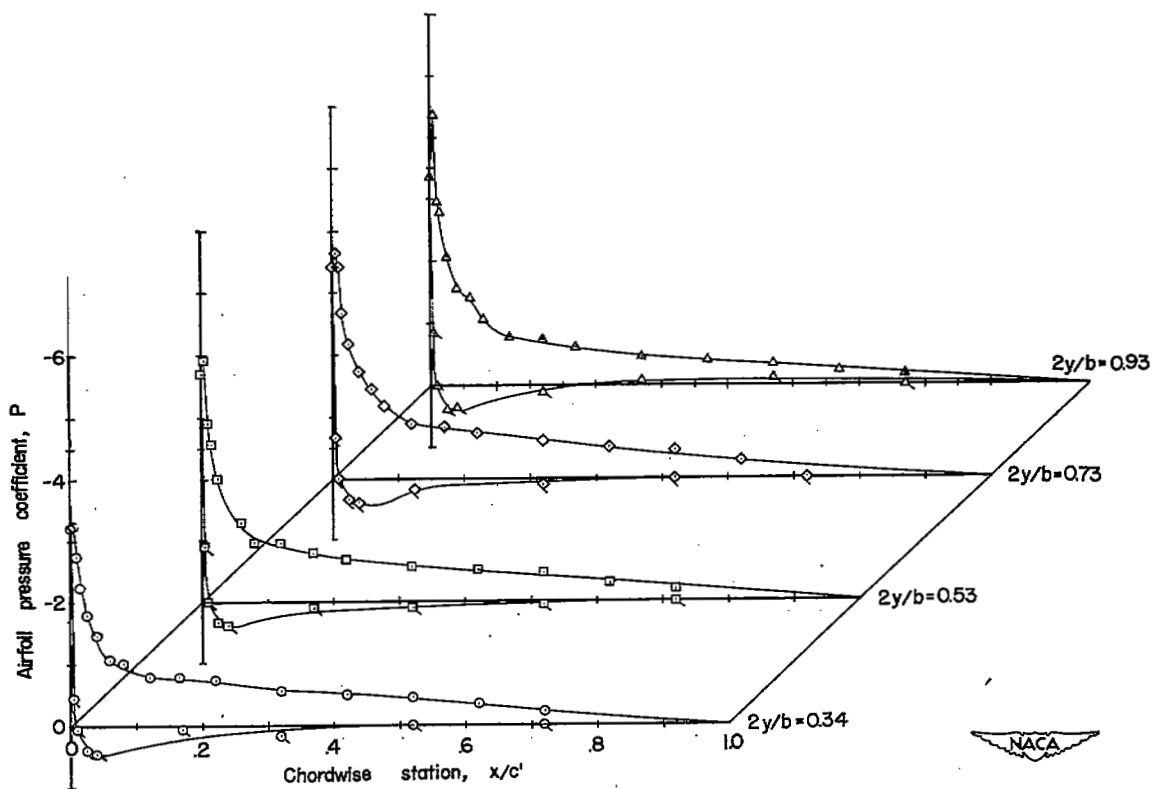
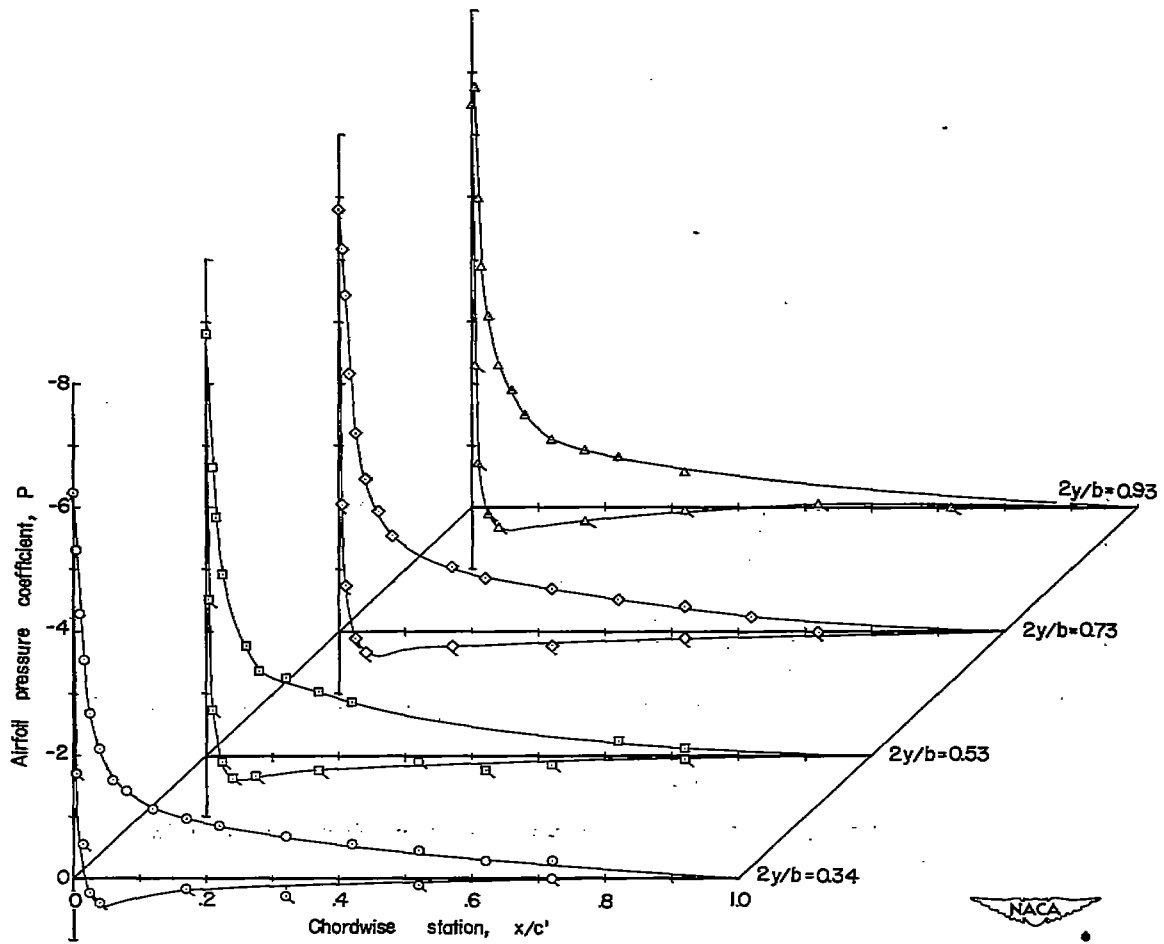


Figure 7.- Effect of spanwise extent of suction on the longitudinal aerodynamic characteristics of a 47.5° sweptback wing-fuselage combination.
 $R = 4.4 \times 10^6$.



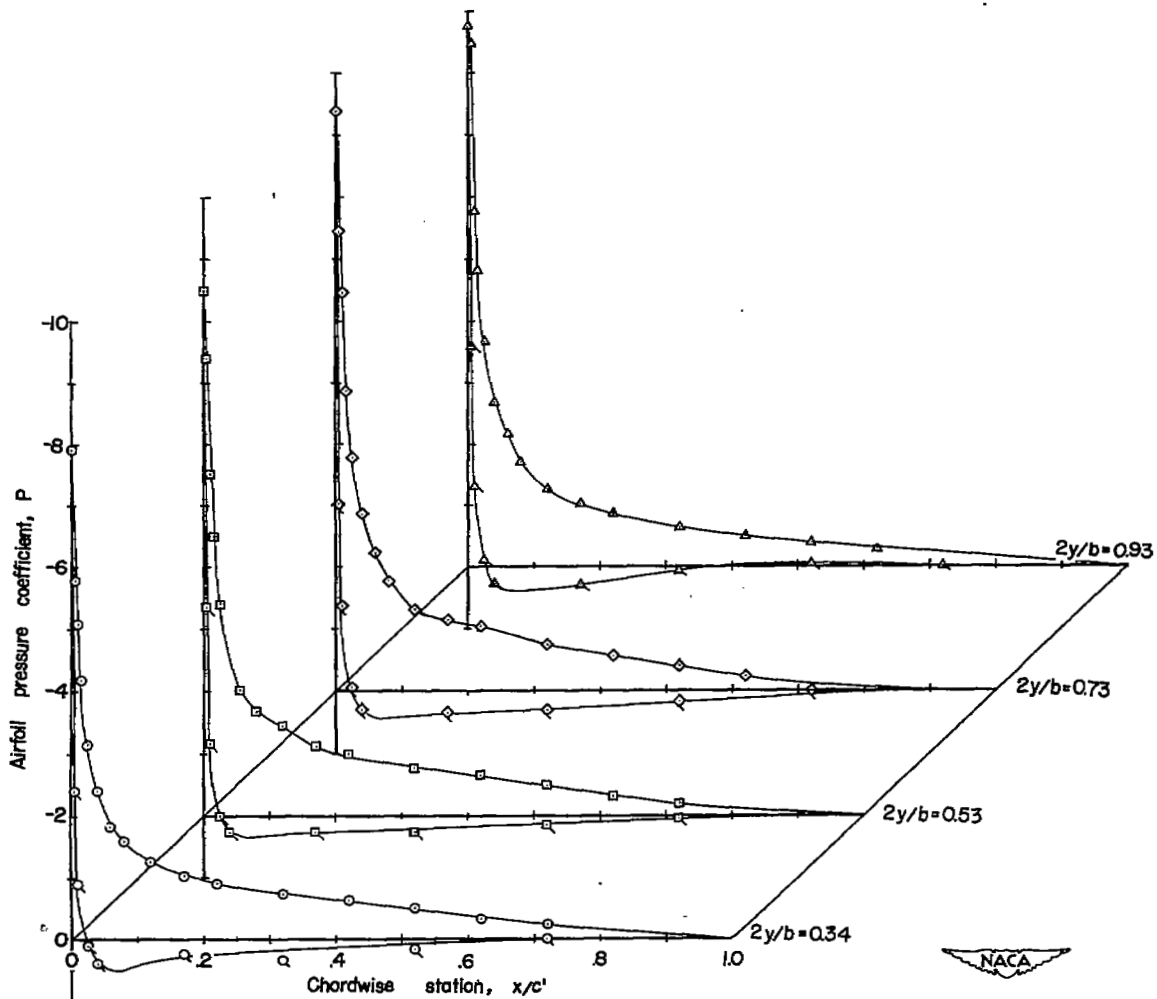
(a) $\alpha = 10.6^\circ$.

Figure 8.- Airfoil pressure distribution over a 47.5° sweptback wing with suction. $0.386\frac{b}{2}\left(0.614 - 1.00\frac{b}{2}\right)$; $0c$ to $0.01c$; $C_Q = 0.00092$; $R = 4.4 \times 10^6$.



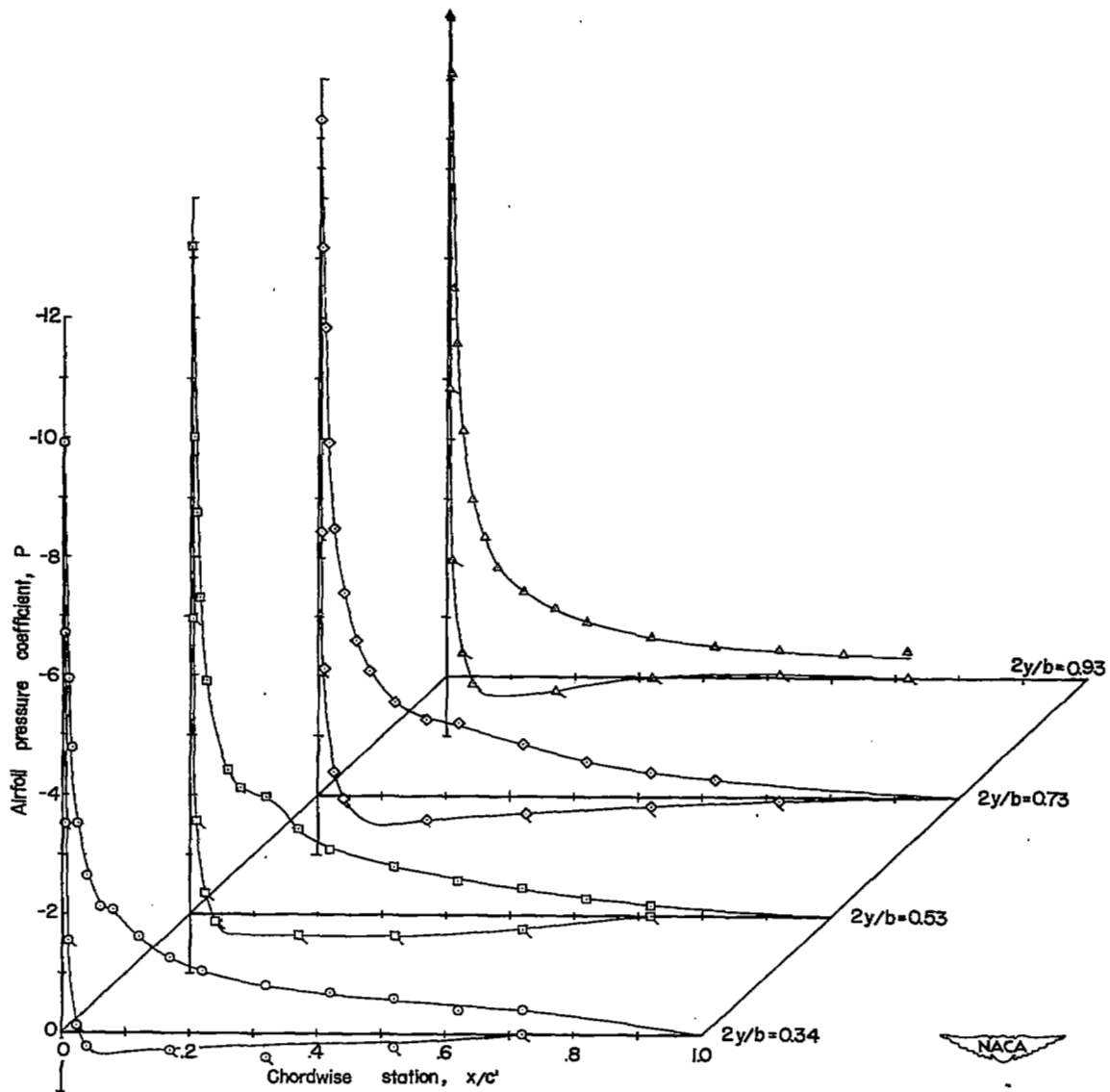
(b) $\alpha = 14.4^\circ$

Figure 8.- Continued.



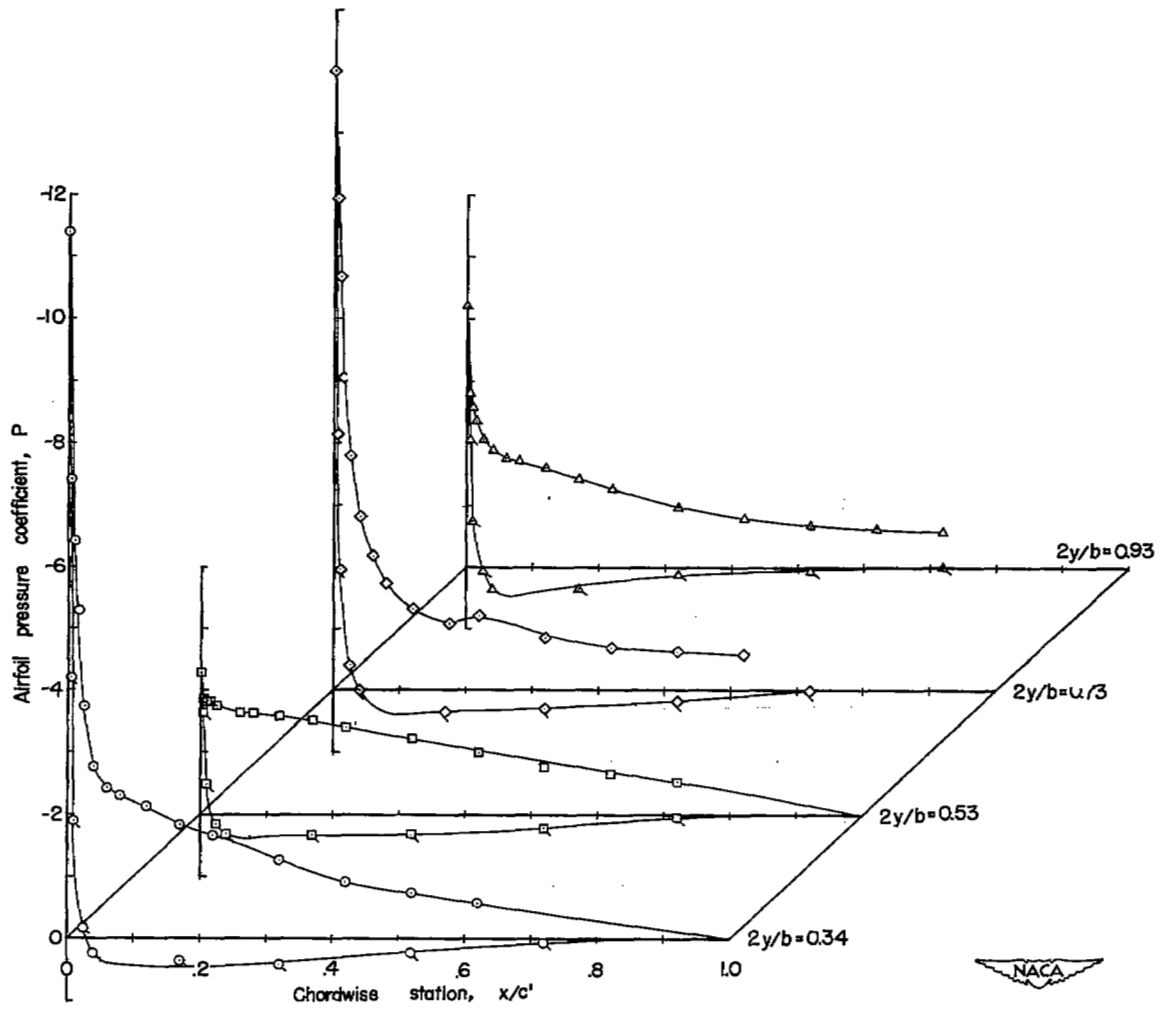
(c) $\alpha = 16.2^\circ$.

Figure 8.- Continued.



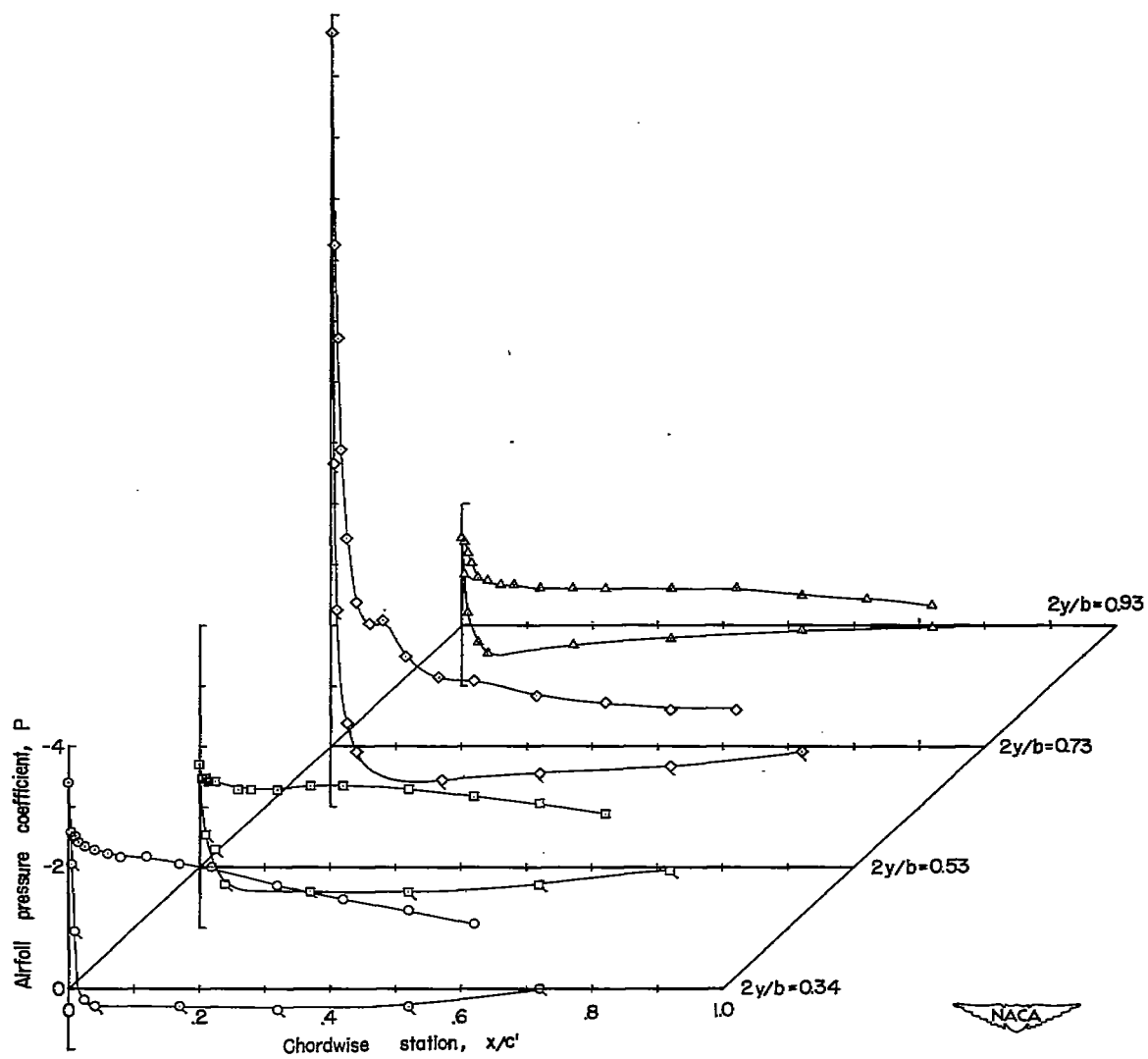
(d) $\alpha = 18.1^\circ$.

Figure 8.- Continued.



(e) $\alpha = 20^\circ$.

Figure 8.- Continued.



(f) $\alpha = 24^\circ$.

Figure 8.- Concluded.

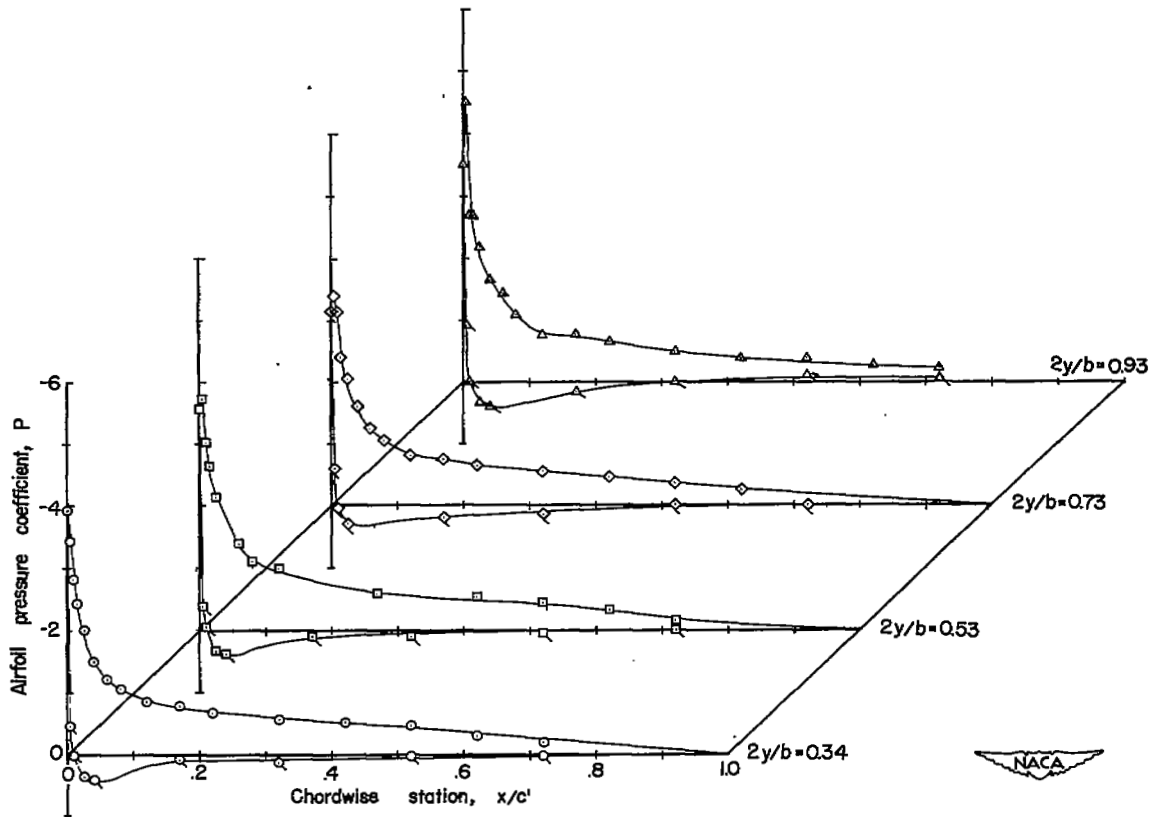
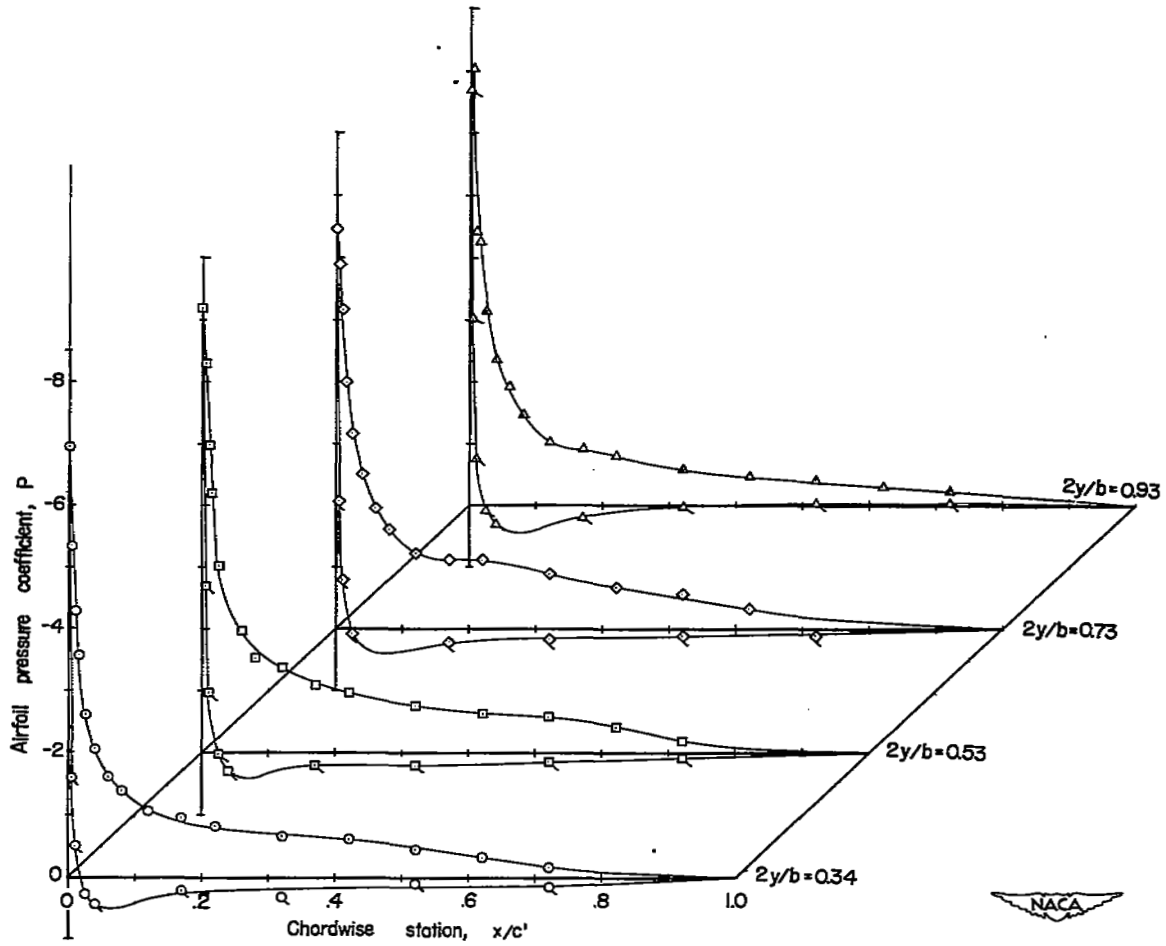
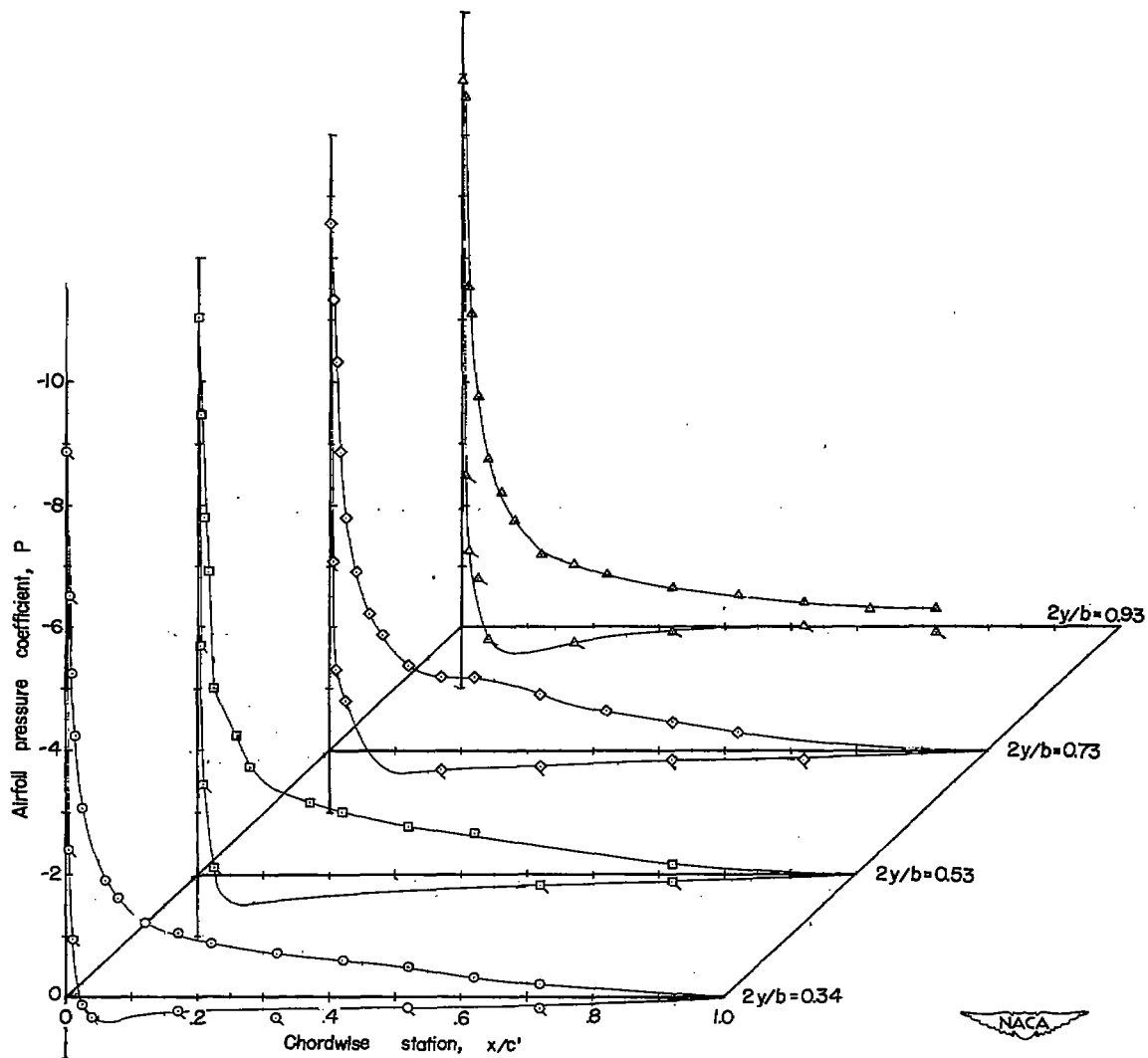
(a) $\alpha = 10.6^\circ$.

Figure 9.- Airfoil pressure distribution over a 47.5° sweptback wing with suction. $0.772\frac{b}{2}$ ($0.228 - 0.614\frac{b}{2}$, $C_Q = 0.00186$; $0.614 - 1.00\frac{b}{2}$, $C_Q = 0.00126$); $0c$ to $0.01c$; $R = 4.4 \times 10^6$.



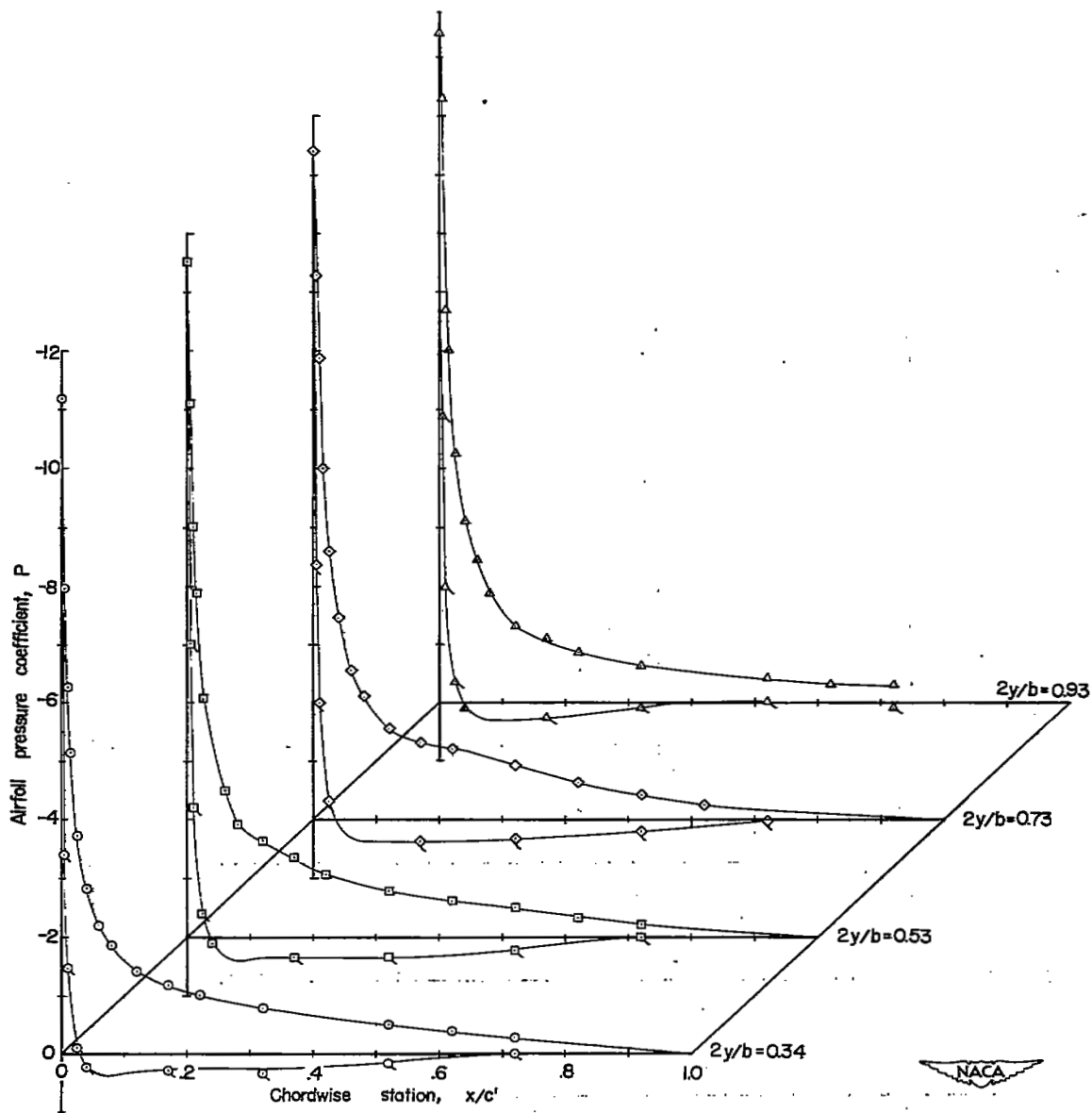
(b) $\alpha = 14.4^\circ$.

Figure 9.- Continued.



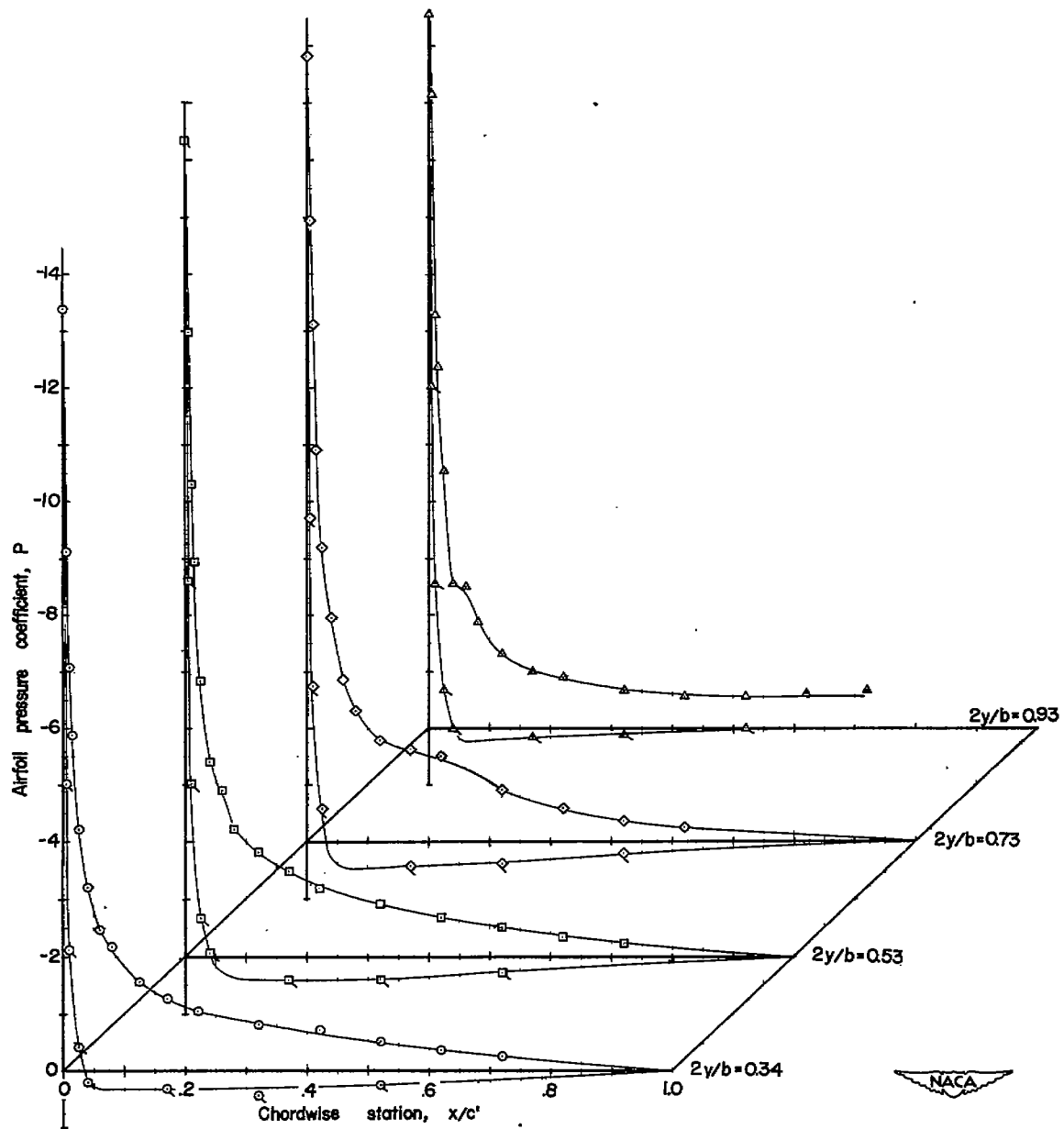
(c) $\alpha = 16.2^\circ$.

Figure 9.- Continued.



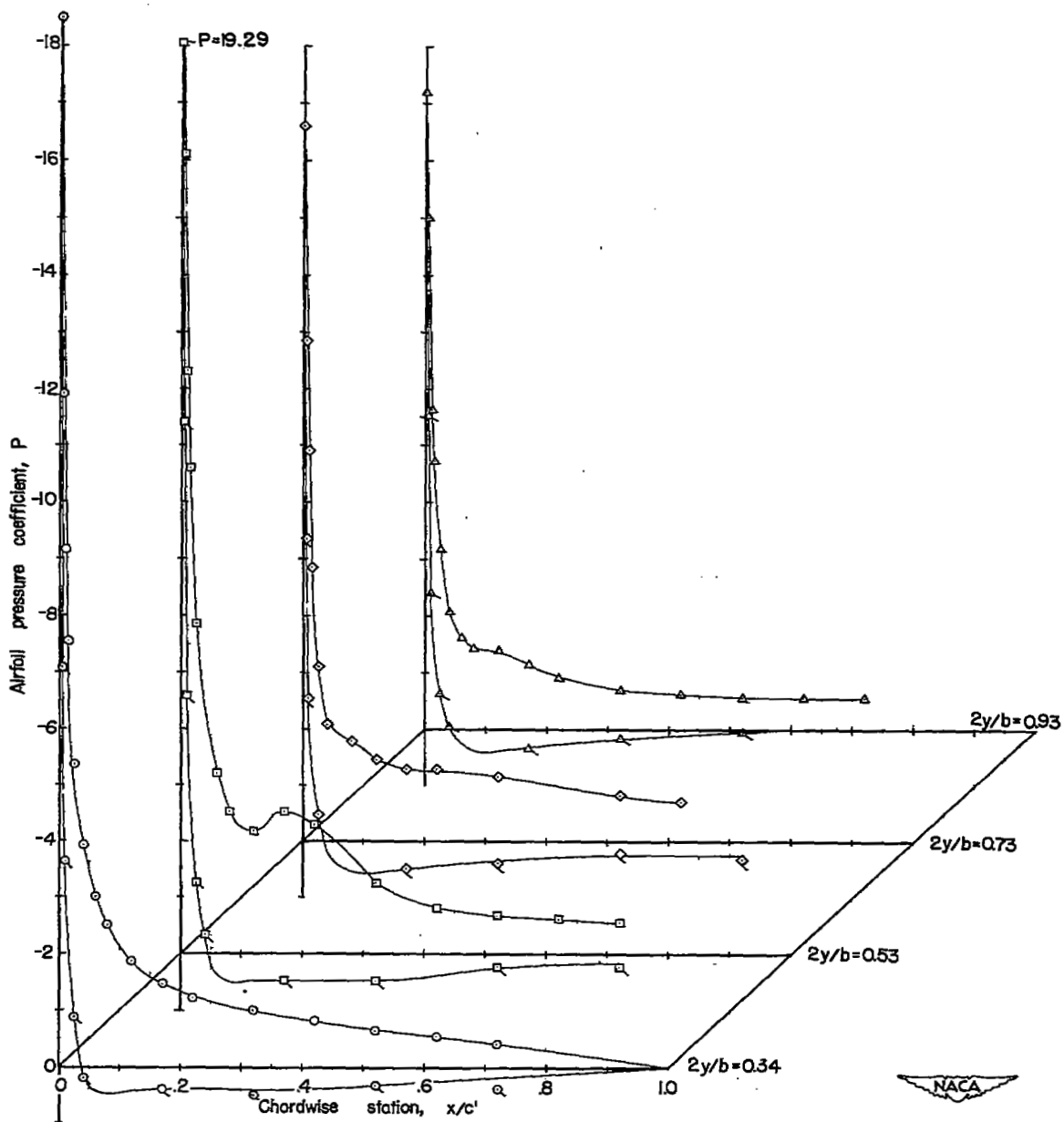
(d) $\alpha = 18.1^\circ$.

Figure 9.- Continued.



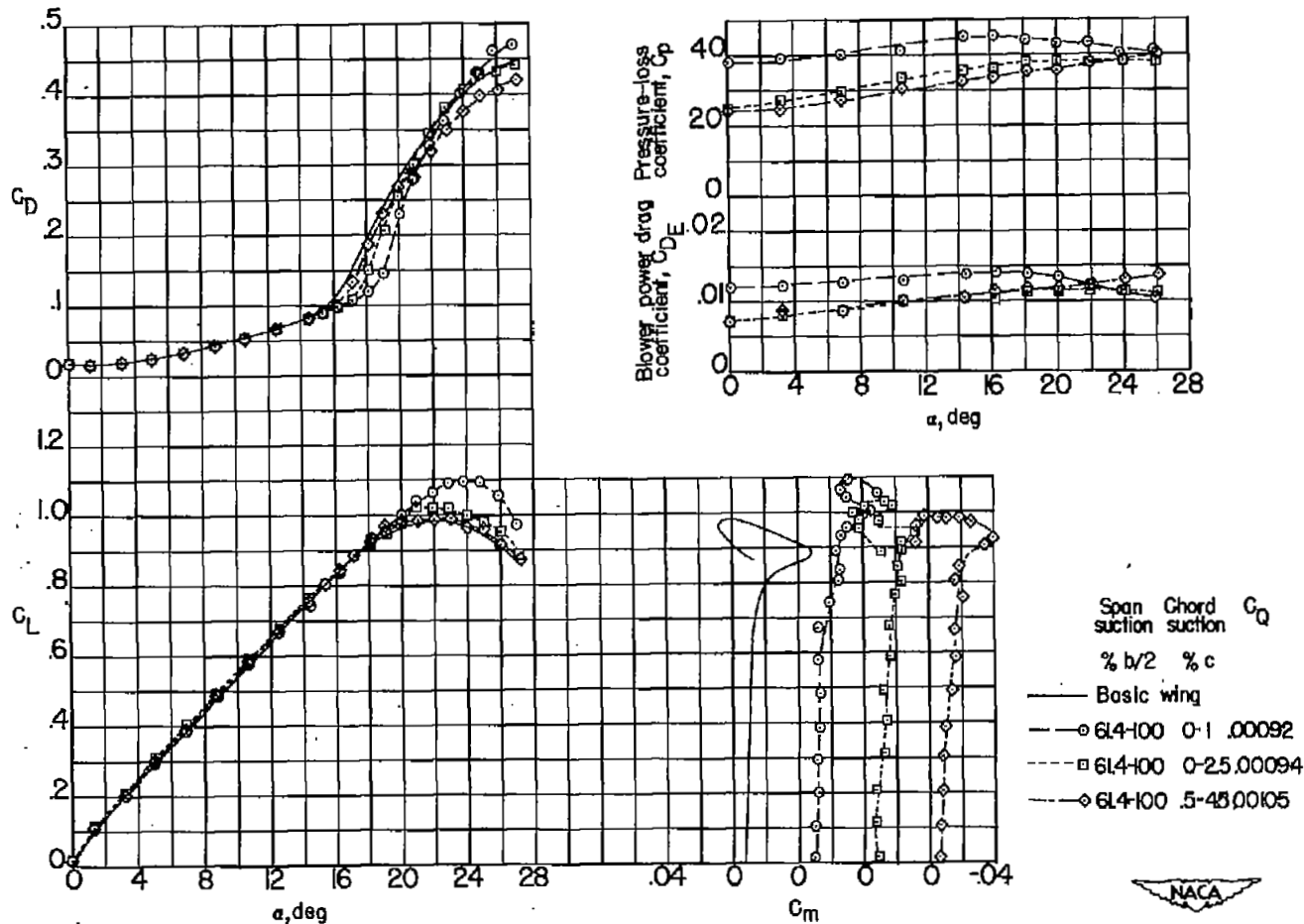
(e) $\alpha = 20^\circ$.

Figure 9.- Continued.



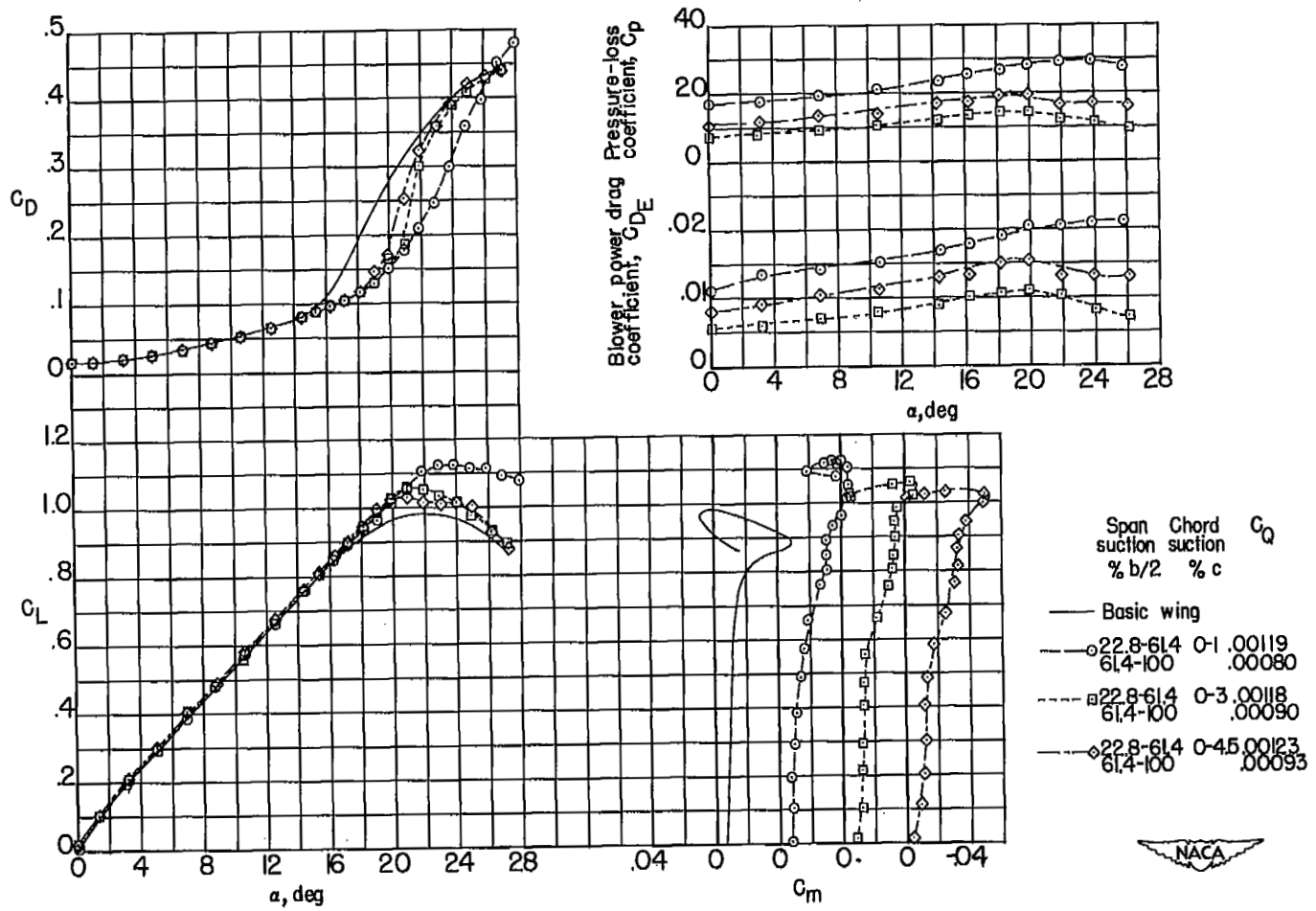
(f) $\alpha = 24^\circ$.

Figure 9.- Concluded.



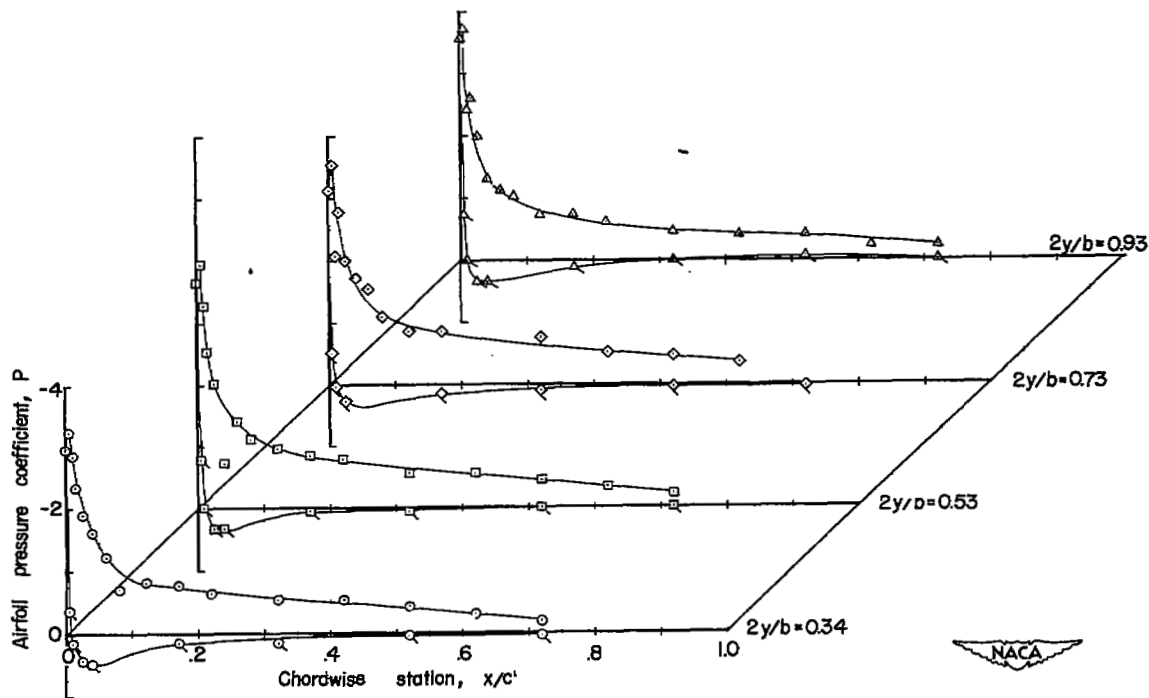
(a) $0.386 \frac{b}{2}$.

Figure 10.- Effect of chordwise extent of suction on the longitudinal aerodynamic characteristics of a 47.5° sweptback wing-fuselage combination. $R = 4.4 \times 10^6$.



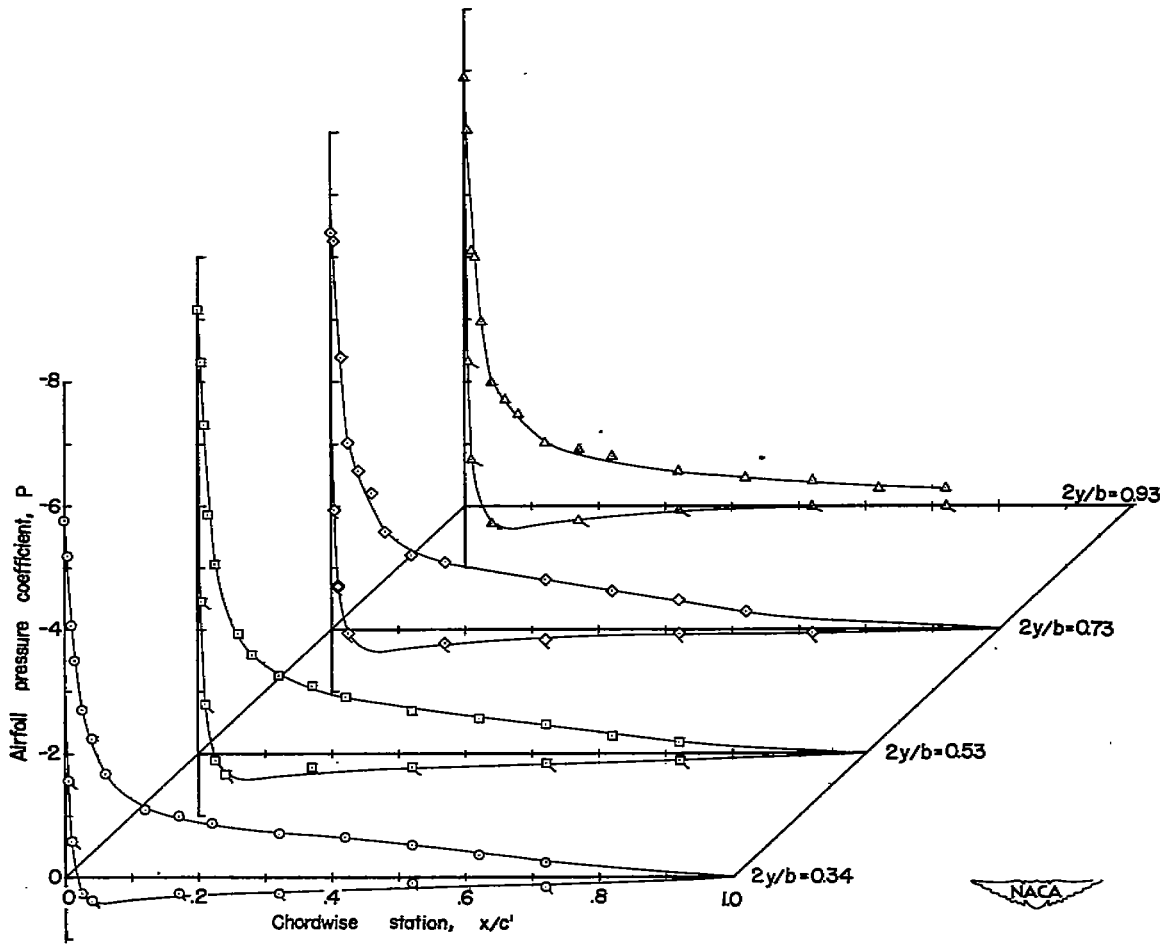
(b) $0.772 \frac{b}{2}$.

Figure 10.- Concluded.



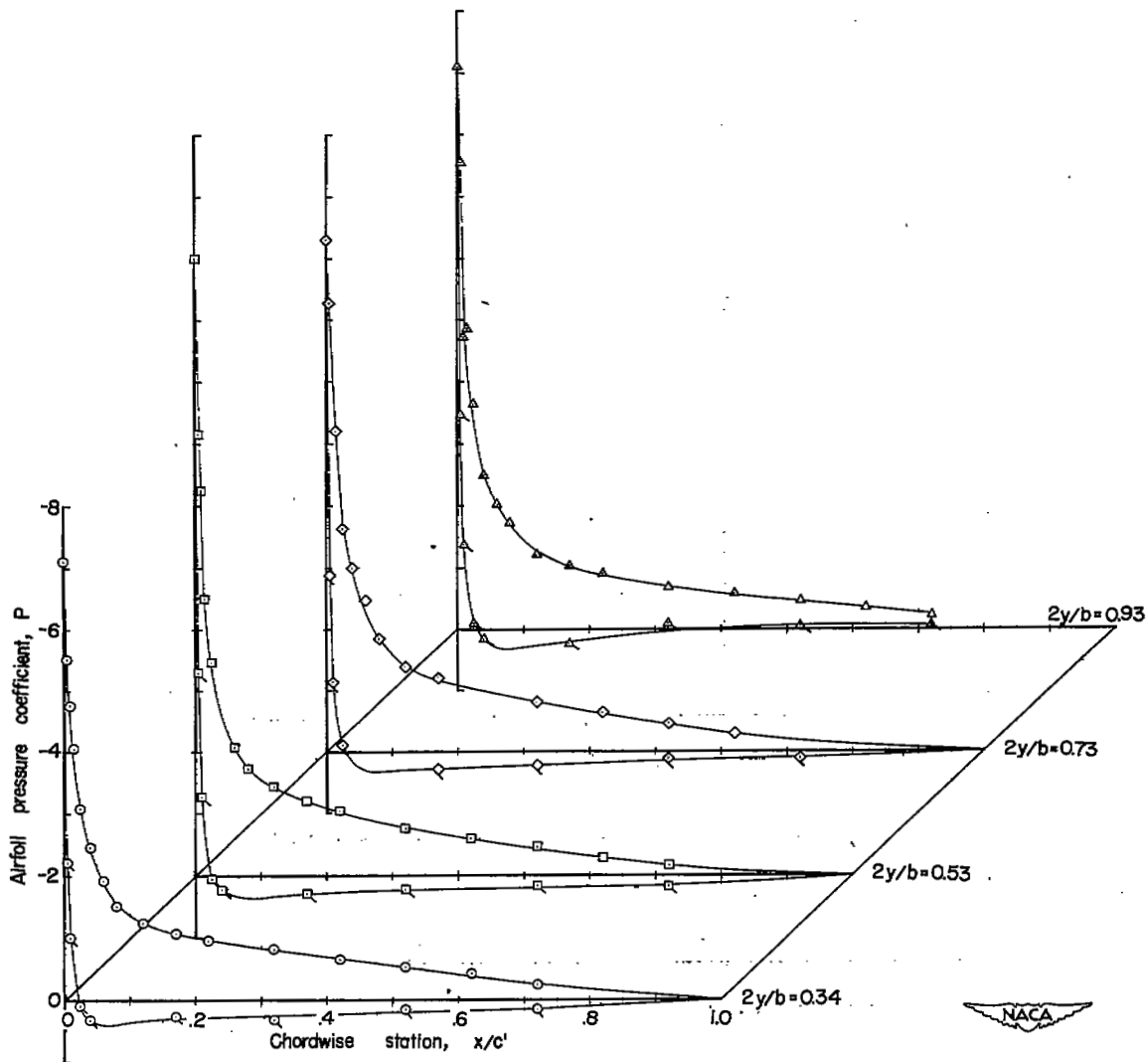
(a) $\alpha = 10.6^\circ$.

Figure 11.- Airfoil pressure distribution over a 47.5° sweptback wing with suction. $0.386 \frac{b}{2} (0.614 - 1.00 \frac{b}{2})$; $0c$ to $0.025c$; $C_Q = 0.00123$; $R = 4.4 \times 10^6$.



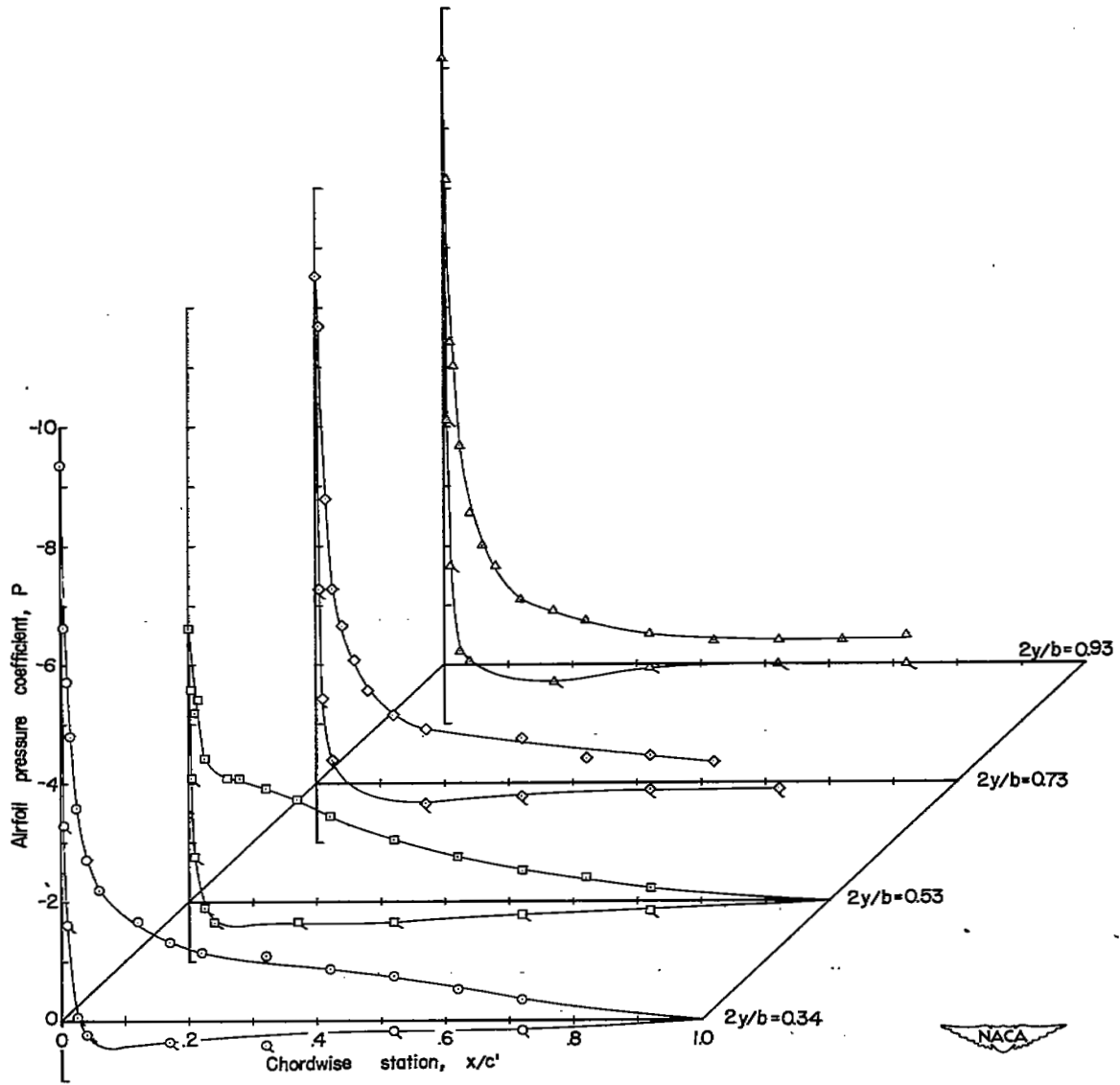
(b) $\alpha = 14.4^\circ$.

Figure 11.- Continued.



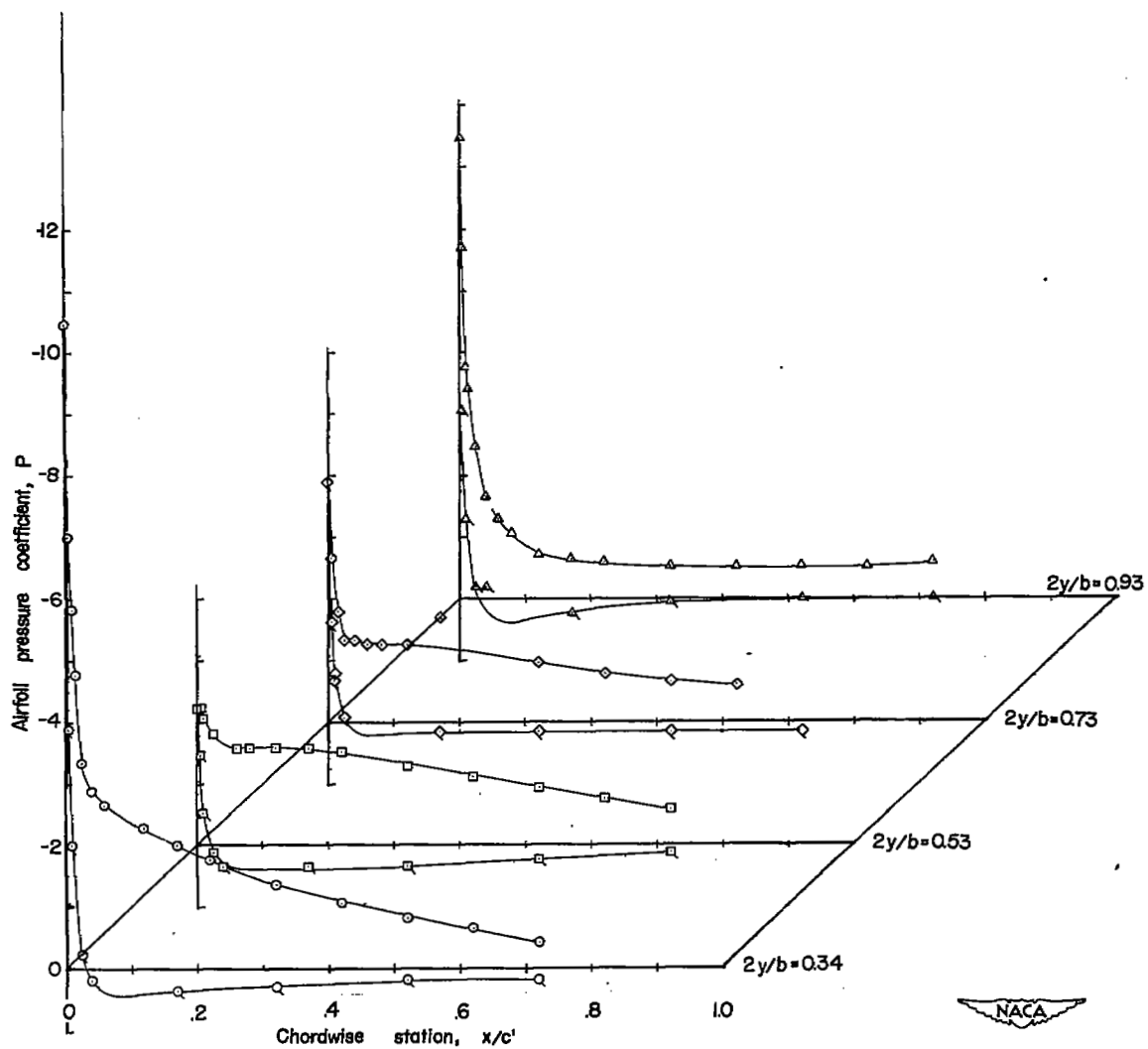
(c) $\alpha = 16.2^\circ$.

Figure 11.- Continued.



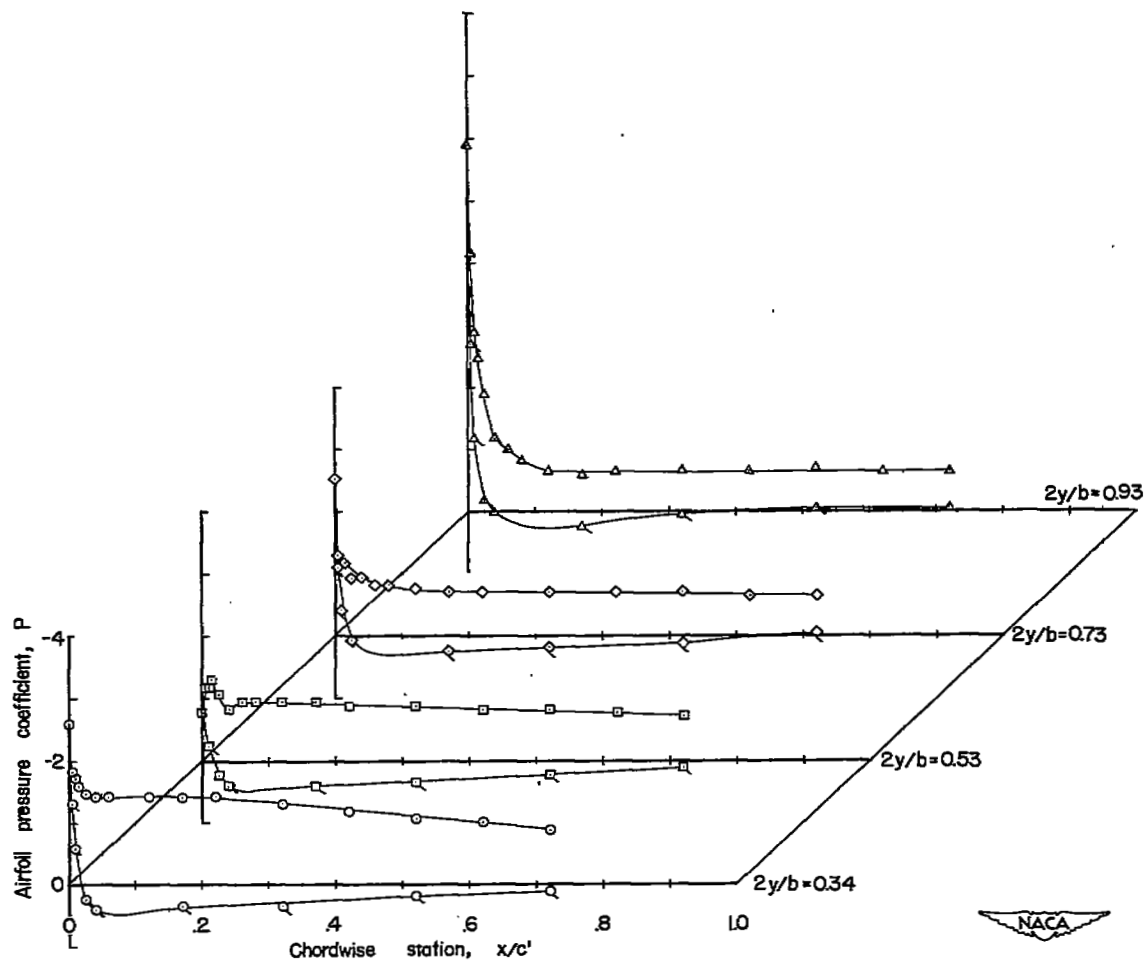
(d) $\alpha = 18.1^\circ$.

Figure 11.- Continued.



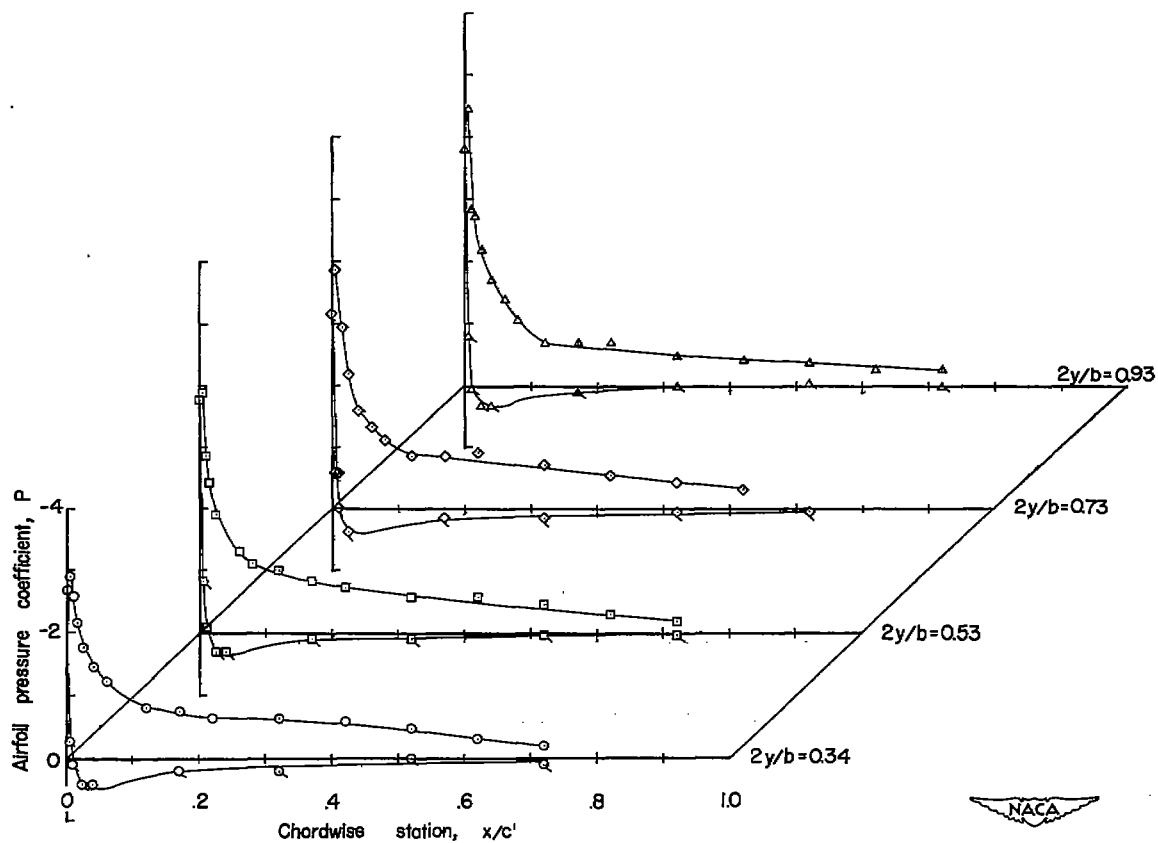
(e) $\alpha = 20^\circ$.

Figure 11.- Continued.



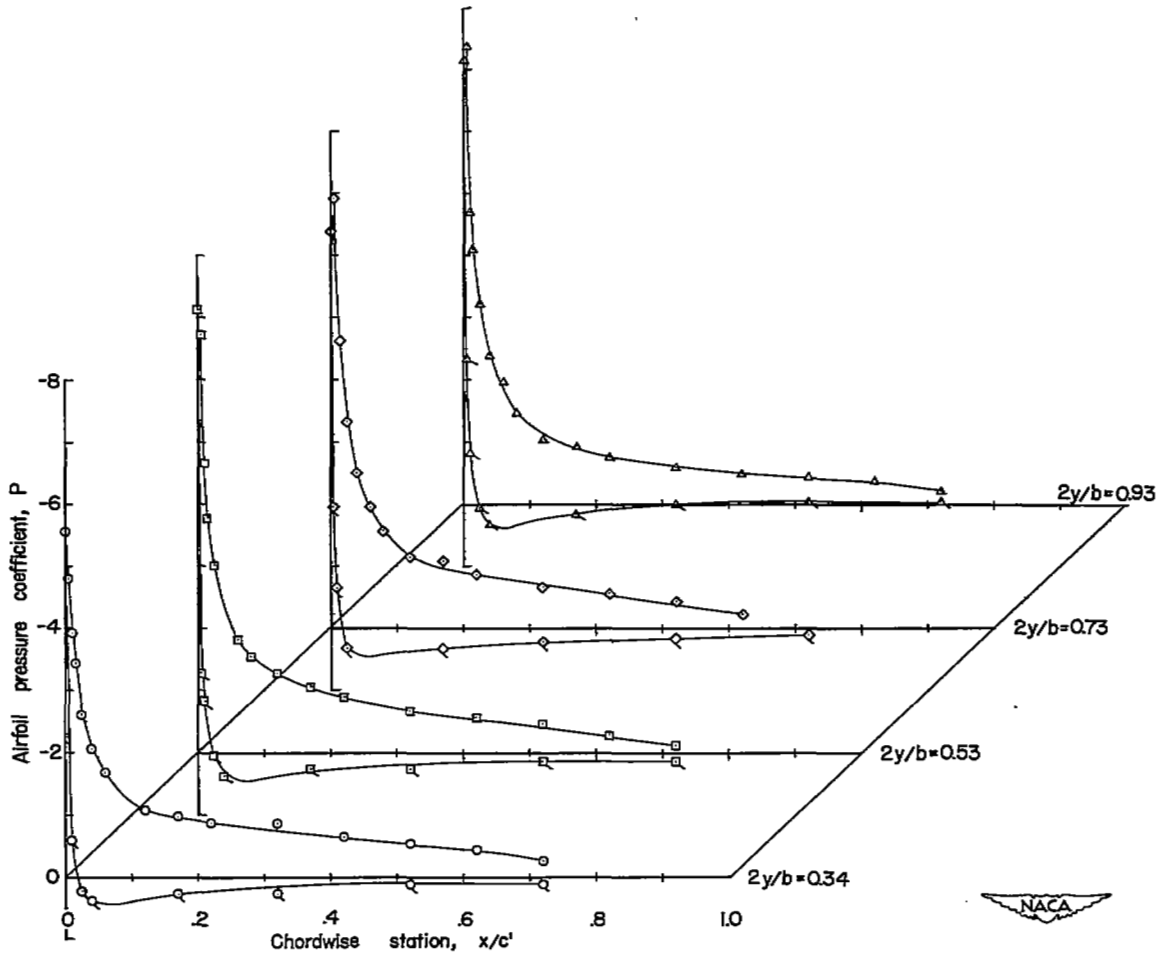
(f) $\alpha = 24^\circ$.

Figure 11.- Concluded.



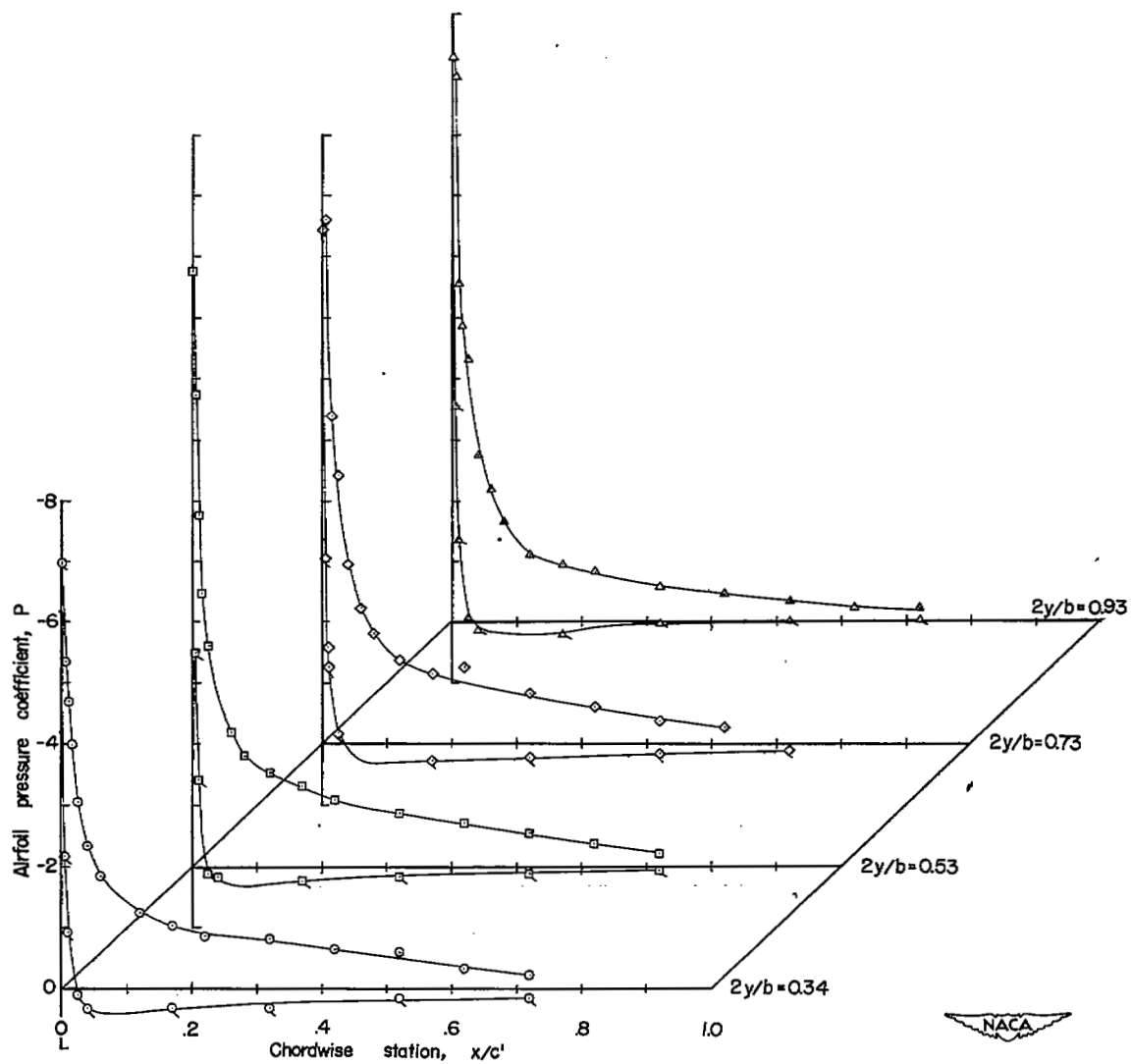
(a) $\alpha = 10.6^\circ$.

Figure 12.- Airfoil pressure distribution over a 47.5° sweptback wing with suction. $0.386\frac{b}{2}(0.614 - 1.00\frac{b}{2})$; $0.005c$ to $0.045c$; $C_Q = 0.00204$; $R = 4.4 \times 10^6$.



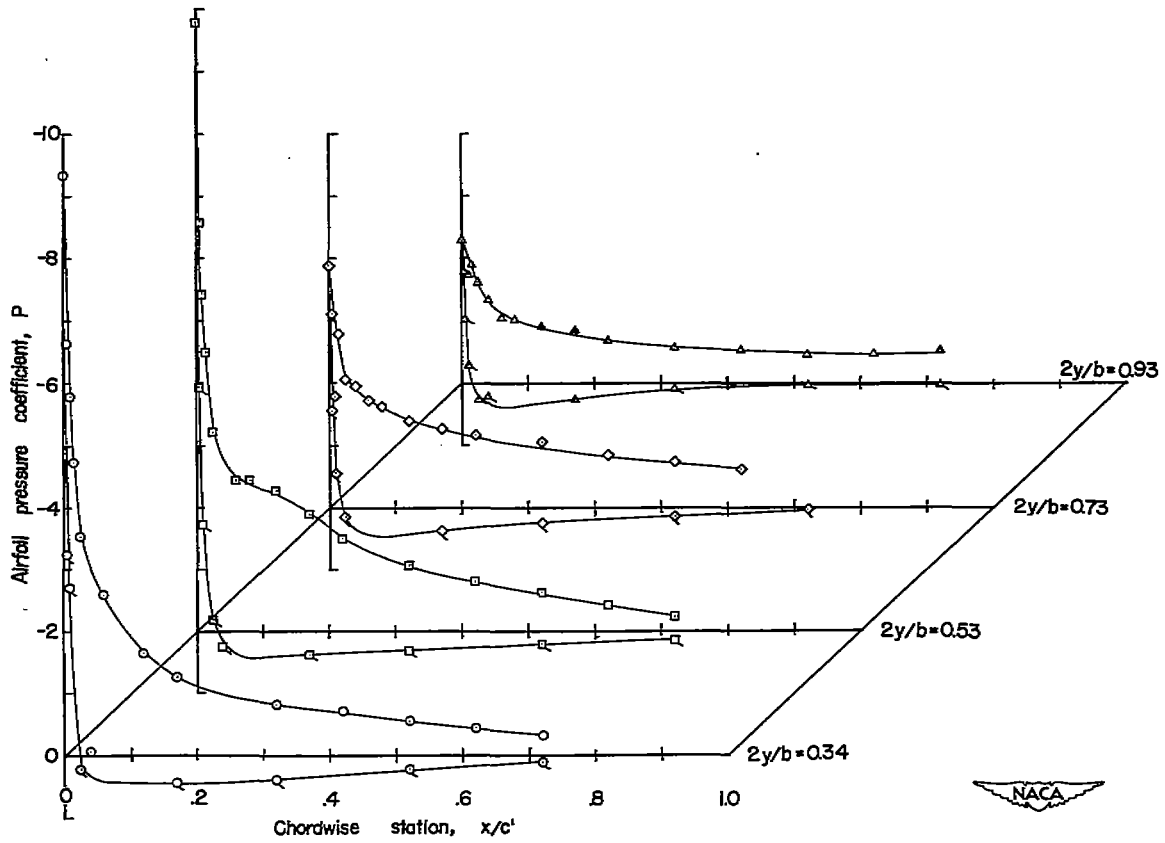
(b) $\alpha = 14.4^\circ$.

Figure 12.- Continued.



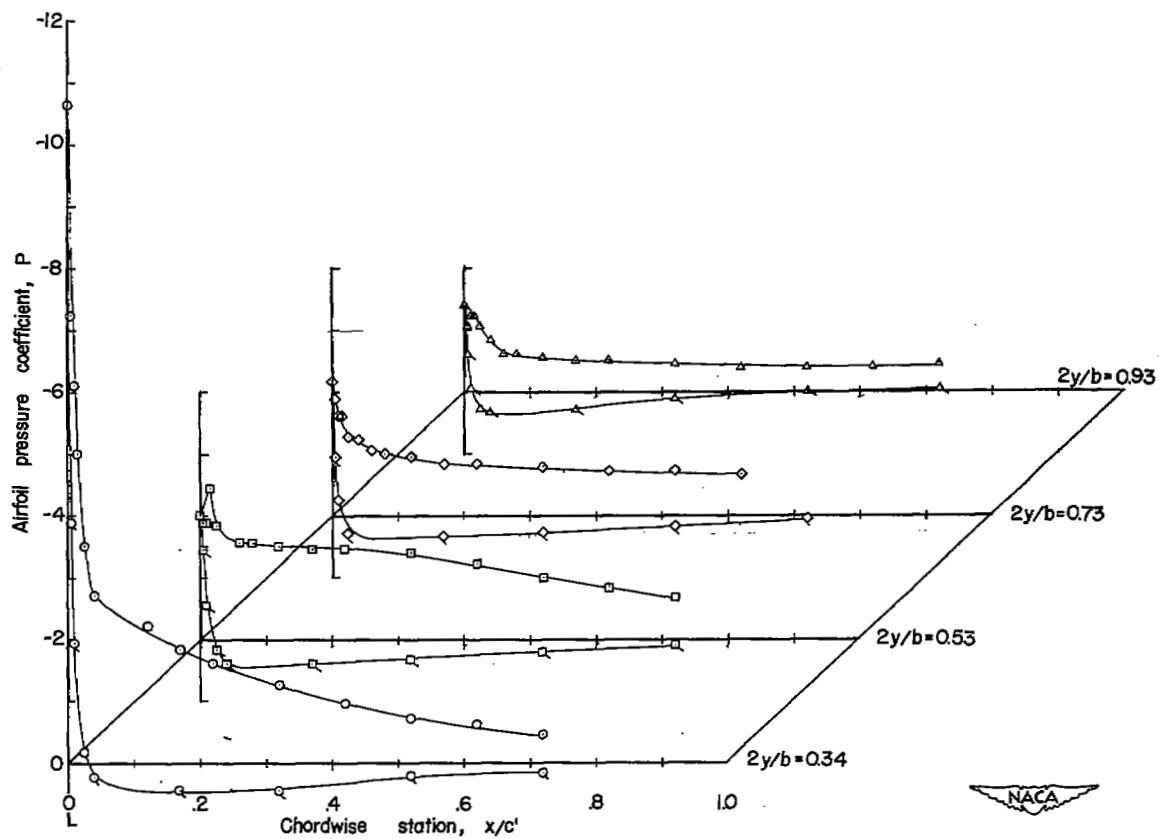
(c) $\alpha = 16.2^\circ$.

Figure 12.- Continued.



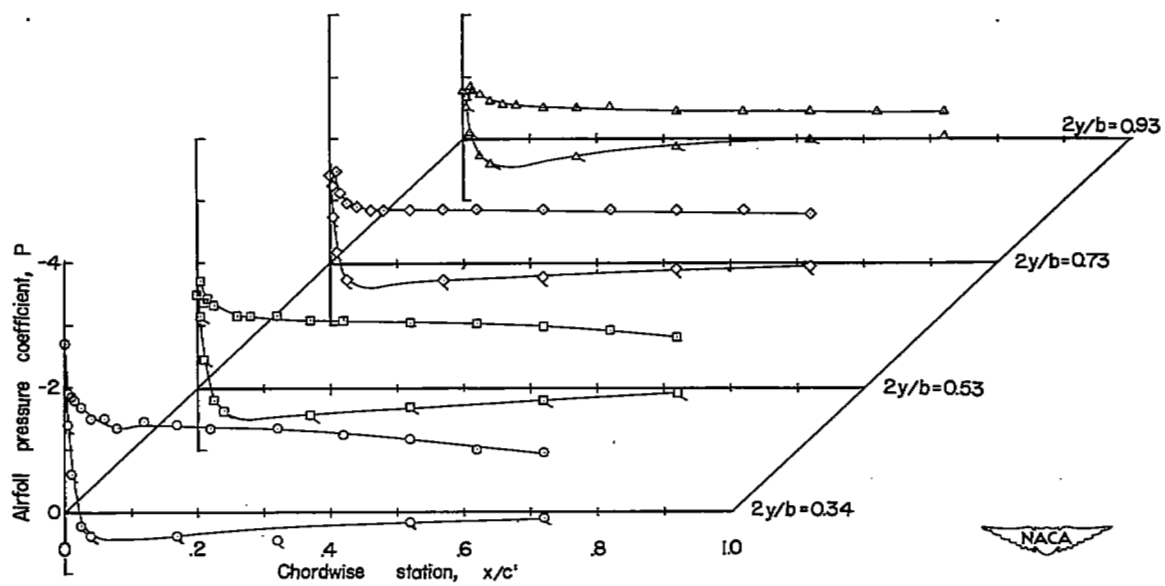
(d) $\alpha = 18.1^\circ$.

Figure 12.- Continued.



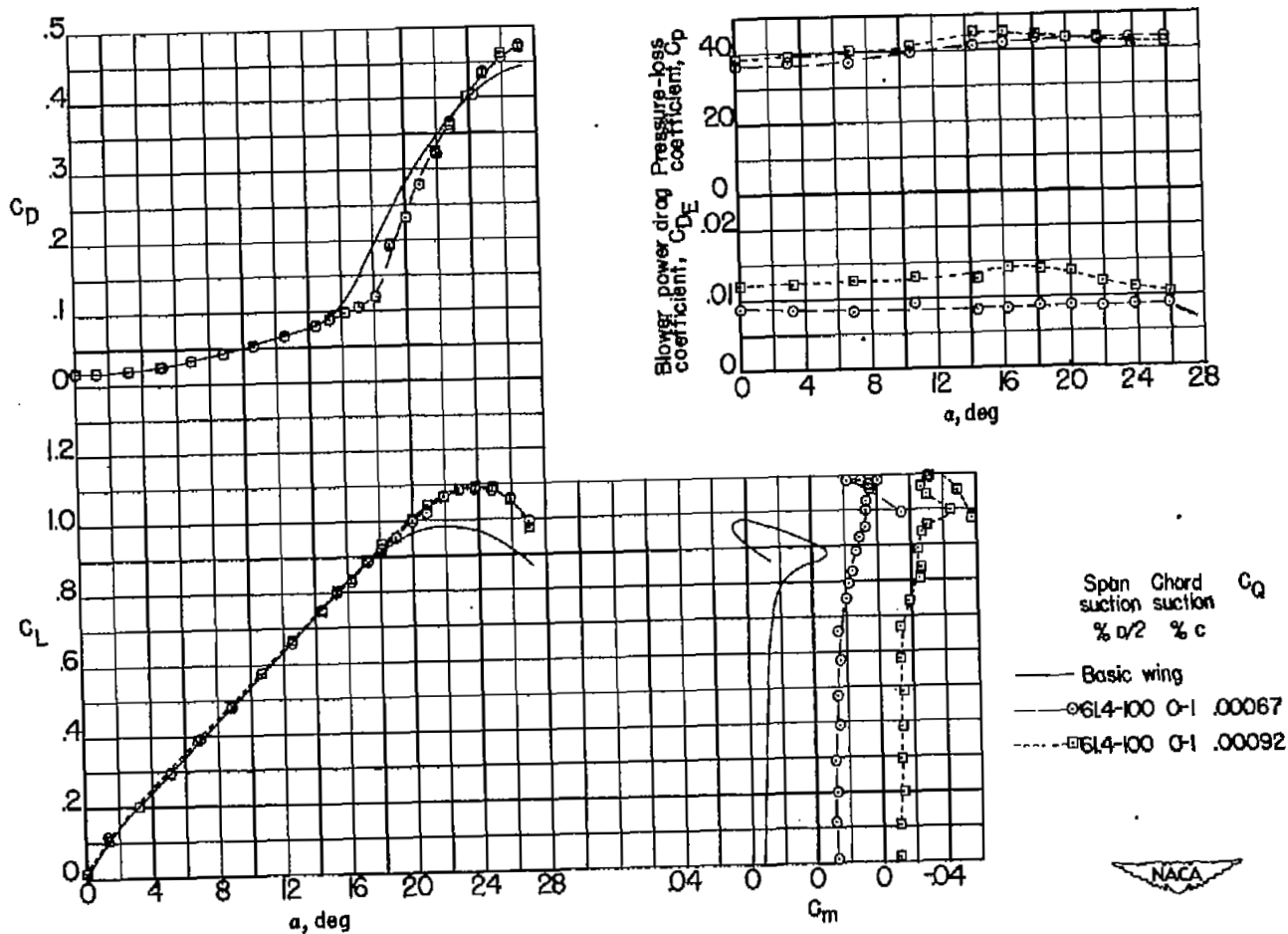
(e) $\alpha = 20^\circ$.

Figure 12.- Continued.



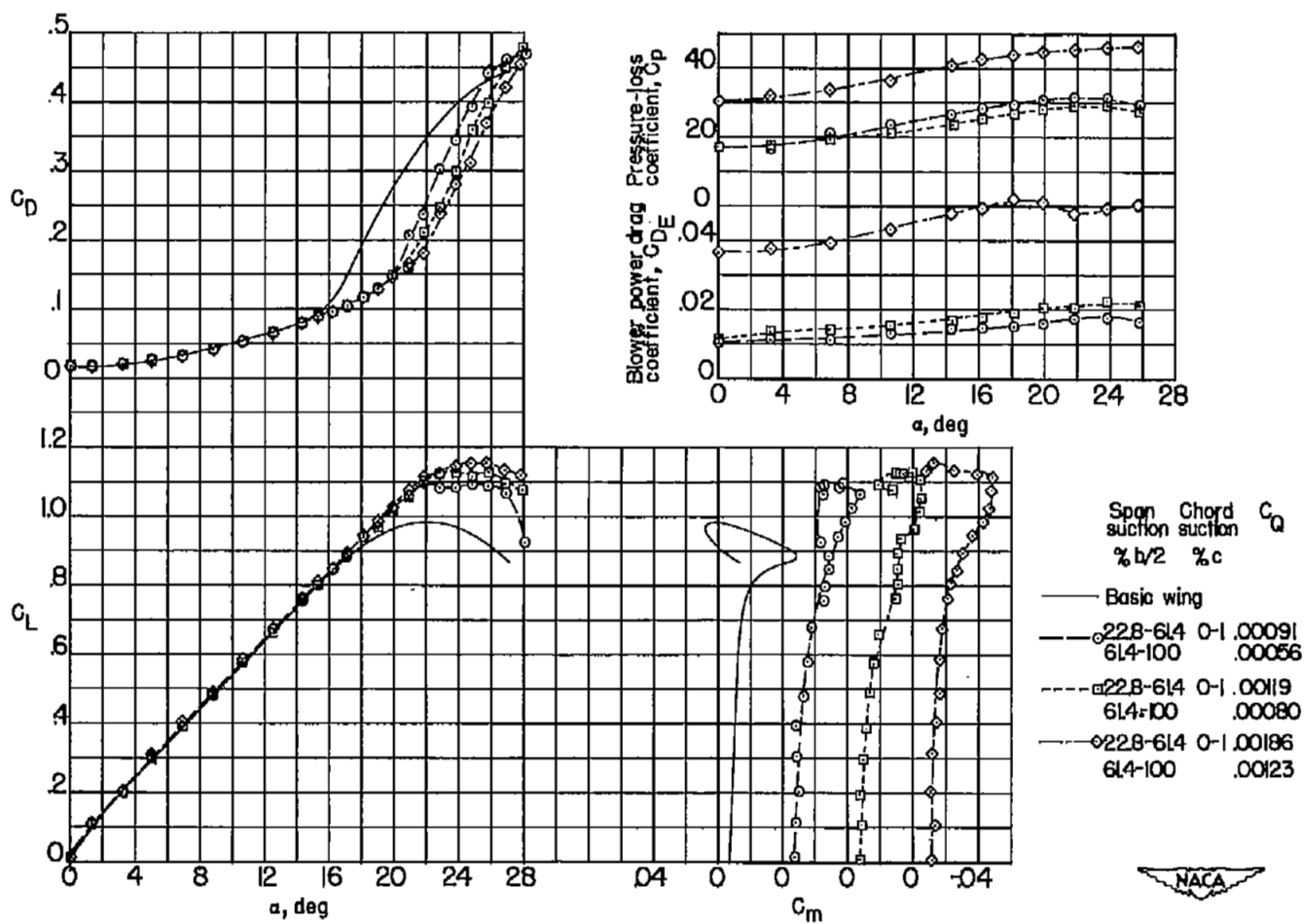
(f) $\alpha = 24^\circ$.

Figure 12.- Concluded.



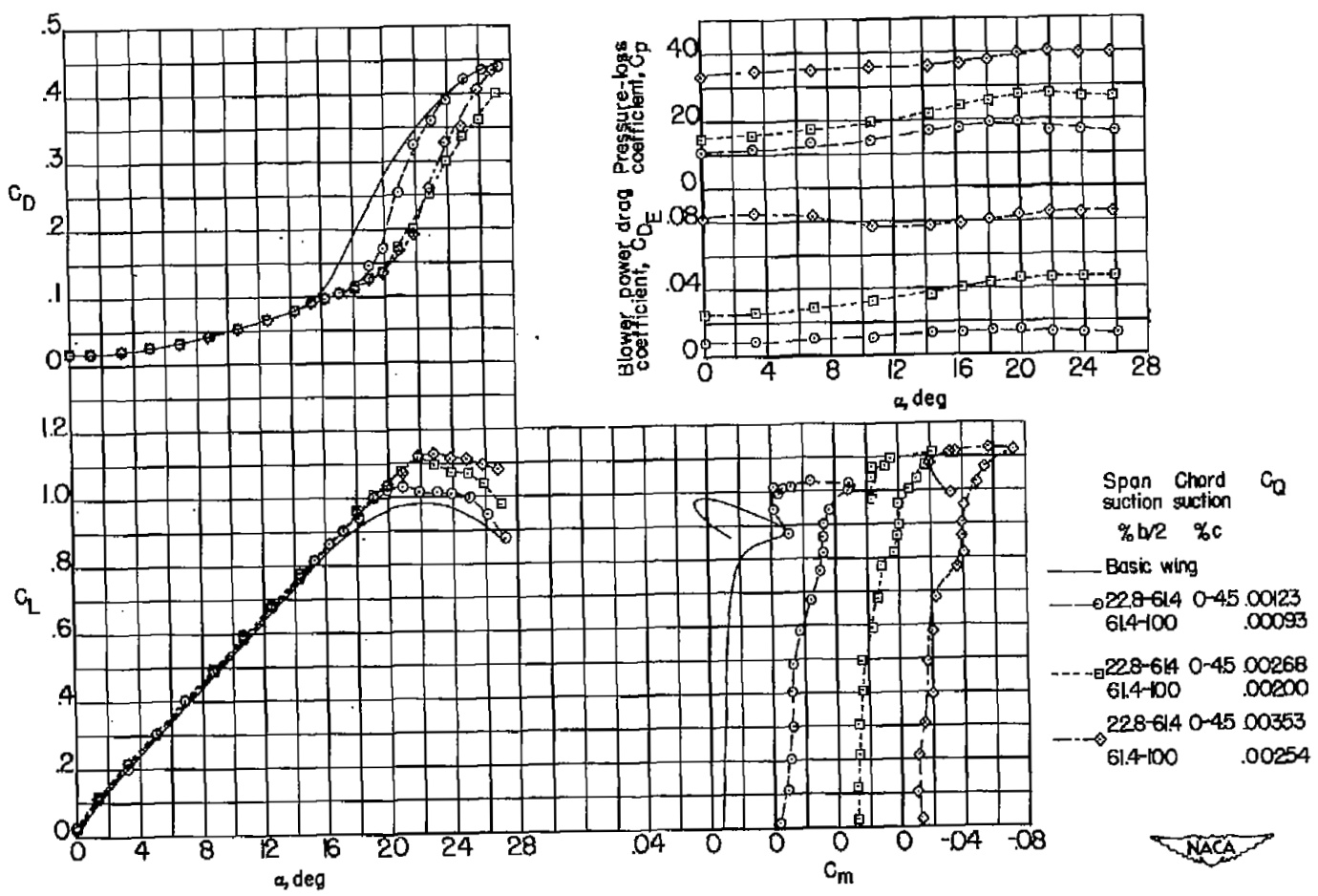
(a) $0.38\frac{b}{2}$; $0c$ to $0.01c$.

Figure 13.- Effect of suction flow rates on the longitudinal aerodynamic characteristics of a 47.5° sweptback wing-fuselage combination.
 $R = 4.4 \times 10^6$.



(b) $0.772 \frac{b}{2}$; $0c$ to $0.01c$.

Figure 13.- Continued.



(c) $0.772 \frac{b}{2}$; $0c$ to $0.045c$.

Figure 13.- Concluded.

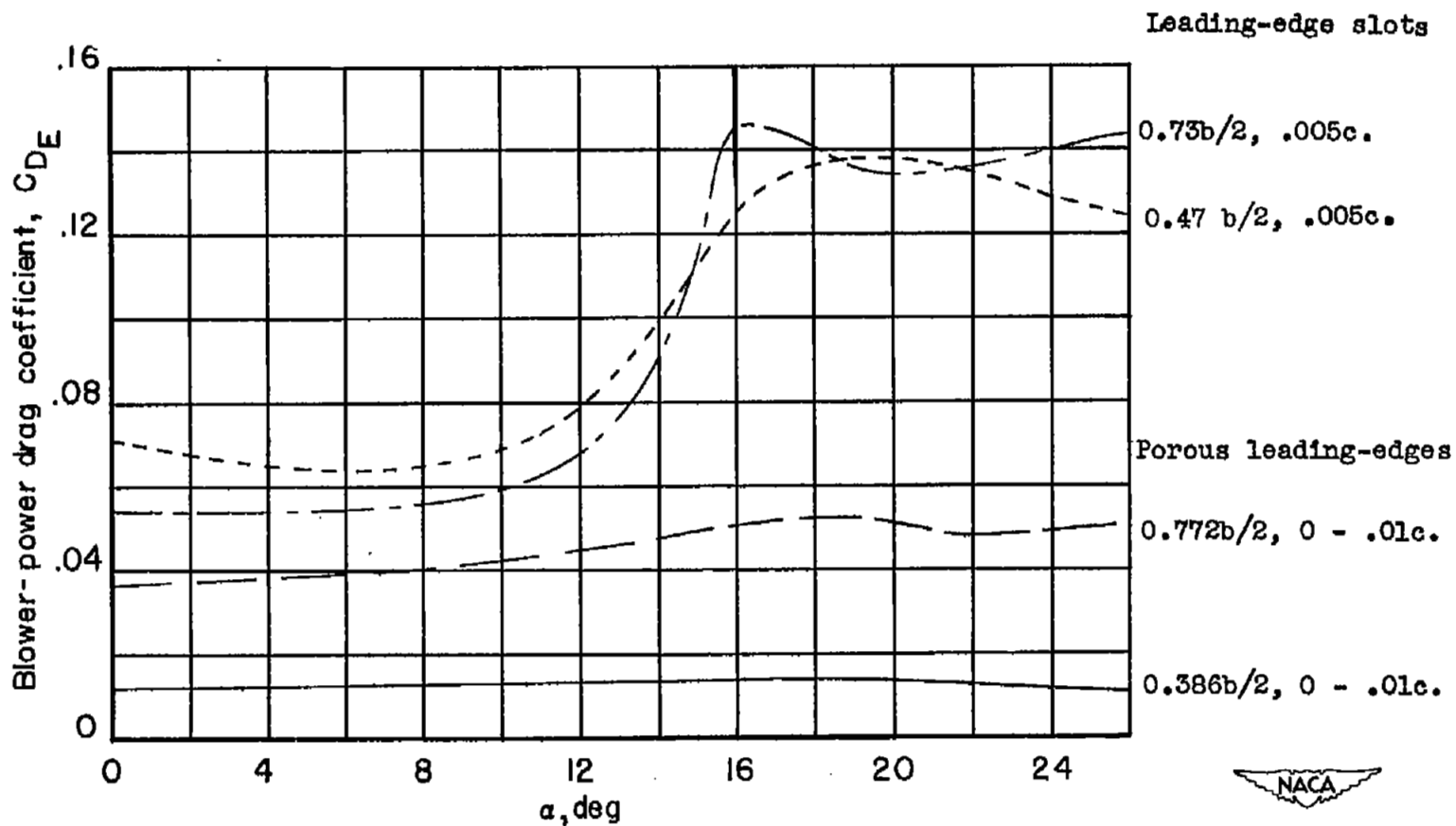


Figure 14.- Comparison of blower power drag of model with suction through porous leading-edge surfaces and leading-edge slots.